

Reactive collisions between electrons and BeT⁺: Complete set of thermal rate coefficients up to 5000 K.

N. Pop¹, F. Iacob^{2,*}, S. Niyonzima³, A. Abdoulanziz⁴, V. Laporta⁵, D. Reiter⁶, I. F. Schneider^{4,7}, and J. Zs Mezei^{8,4}

¹*Department of Physical Foundations of Engineering,*

Politehnica University of Timisoara, 300223 Timisoara, Romania

²*Department of Physics, West University of Timisoara, 300223 Timisoara, Romania*

³*Département de Physique, Fac. des Sciences, Université du Burundi, B.P. 2700 Bujumbura, Burundi*

⁴*LOMC CNRS-UMR6294, Université le Havre Normandie, F-76058 Le Havre, France*

⁵*Istituto per la Scienza e Tecnologia dei Plasm, CNR, 70126 Bari, Italy*

⁶*Institute for Laser and Plasma Physics, Heinrich-Heine-University, D-40225 Düsseldorf, Germany*

⁷*LAC CNRS-FRE2038, Université Paris-Saclay, F-91405 Orsay, France and*

⁸*Institute for Nuclear Research (ATOMKI), H-4001 Debrecen, Hungary*

(Dated: March 9, 2022)

Rate coefficients for the dissociative recombination, vibrational excitation and vibrational de-excitation of the BeT⁺ ion for all vibrational levels of its ground electronic state ($X^1\Sigma^+, v_i^+ = 0, \dots, 27$) are reported, including in the calculation the contribution of super-excited states of the BeT complex pertaining to three electronic symmetries - $^2\Pi$, $^2\Sigma^+$, and $^2\Delta$. These data are suitable for the kinetic modeling of beryllium and tritium containing plasma, as encountered in magnetic fusion devices with beryllium walls (JET, ITER). In the present study we restrict ourselves to incident electron energies from 10^{-3} up to 2.7 eV, and to electron temperatures between 100 and 5000 K, respectively. Together with our earlier and closely related studies on the BeH⁺ and BeD⁺ systems, this present work completes the isotopic coverage for the beryllium monohydride ions. The vibrational energy (rather than the vibrational quantum state) is identified as a proper isotopic similarity parameter, e.g., for reduced but still isotopically correct plasma chemistry models.

I. INTRODUCTION

The plasma in the peripheral region (plasma boundary) of the ITER fusion reactor [1] necessarily interacts with the first wall materials, which are mostly covered with the low Z metal beryllium in the main chamber. In the outer (near wall) plasma domains this leads to a complex diversity of interconnected physical and chemical elementary processes [2]. The fuel used in the activated phases in next step magnetic fusion reactors consists of deuterium and the tritium at equal concentrations. The d-t fusion reaction leads to helium and neutrons as products, which carry the excess energy from these fusion processes as kinetic energy. While the neutrons leave the plasma flame, the helium ash is confined and therefore magnetically guided out (together with the other plasma constituents) from the main plasma chamber into the so called divertor [1, 2]. The latter is equipped with pumps and high heat flux components (currently envisaged there: tungsten target surfaces).

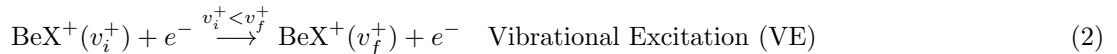
Beryllium and tungsten are therefore considered as major plasma-facing materials for the ITER reactor [3–5] which, once released, act as plasma impurities. Thus it is of great importance to quantitatively understand their release, the transport, and the chemical reactivity of these metals in the plasma. The main chamber beryllium wall is exposed to plasma heat and particle bombardment from the outer boundary plasma region. Identification and quantification of the various release candidate mechanisms, such as physical, chemical sputtering or other such processes, is still an active field of ongoing research in magnetic confinement fusion [3, 6, 7]. Chemically assisted physical sputtering contributes to the formation of beryllium atoms at surfaces; release mechanisms of molecular forms BeH or BeH₂ may also play a role. The beryllium atoms or beryllium hydrides in turn will enter into the plasma, fragment (dissociate) and radiate there, and/or form further molecular species like BeH, BeD and BeT (or their ions) in chemical reactions with the atoms of the fuel (H, D, T) or their molecules.

Besides the experimentally confirmed presence of Be containing neutral atomic and molecular species in magnetic fusion plasma, their ionic counterparts (Be⁺, BeX⁺, where X stands for H, D, or T) were also presumed early [8–10] and meanwhile also been experimentally confirmed by spectroscopic methods [11–15]. Even though the fuel hydrogen isotopes remain, by far, the dominant gas and charged components, in the colder edge/divertor regions collisions between comparatively low energy (0.1 – 100 eV) electrons and BeX⁺ ions can play a significant role for the overall transport and fragmentation pathways of these impurities and hence, globally, for the fusion plasma flame purity. Typically, in current fusion devices related impurity wall release rates are inferred only rather indirectly, via intensity of light emission from the Be and BeX containing plasma constituents. However, this experimental procedure combines

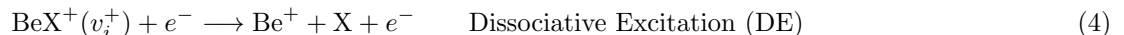
*felix.iacob@e-uvt.ro

two unknowns: firstly the surface release mechanisms and rates, and, secondly, the (mostly) electron collision driven volumetric collisional processes (incl. fragmentation, excitation, etc.). Our present computational work on the BeX^+ family of ions contributes to a wider effort to separate these two unknowns, by isolating the latter with detailed theoretical cross section calculations, hence to make the former then better experimentally accessible.

The most relevant reactive collisions starting from BeX^+ ions that can take place are the following:



and, at high collision energies - which will be a range addressed in future work:



where v_i^+ and v_f^+ denote the initial and final vibrational quantum numbers of the target cation.

In the framework of the Multichannel Quantum Defect Theory (MQDT) [16–21] we have performed nuclear dynamics calculations using previously computed molecular data [20, 22] updated for the heaviest beryllium monohydride isotopologues. The present work continues and ends a series of studies we performed on the DR, VE and VdE - eqs. (1-3) - of BeH^+ [10, 20, 23] and BeD^+ [24–26] with electrons of low to moderate collision energy. Here we first present a complete study on the vibrational dependence of the DR, VdE and VE rate coefficients of BeT^+ cation. Having thus completed the set of monohydride BeX^+ ion isotopologues enables us now to also derive an isotopic scaling law from this data-set (see Section 3), which greatly facilitates the use of this detailed information inside the physically and numerically already demanding multi-physics multi-scale fusion boundary plasma computational tools, such as the current ITER boundary plasma suite of codes SOLPS-ITER [27].

The paper is organized as follows: The introduction is followed by a brief description of the employed theoretical approach and some computational details. Section III presents our calculated rate coefficients. The paper ends with conclusions.

II. THEORETICAL APPROACH OF THE DYNAMICS

In the present study, we used an MQDT-based method to study the electron-impact collision processes given by Eqs. (1–3). Along with other methods we use [28], MQDT has proven to be a powerful and successful method when applied to several diatomic systems like H_2^+ [29], N_2^+ [30], CO^+ [31]. This approach, combined with the R-matrix technique, was also used to model satisfactorily - although less accurately - electronic collisions with poly-atomic ions like BF_2^+ [32] and $\text{NH}_2\text{CH}_2\text{O}^+$ [34].

The processes studied in the present paper involve ionization channels, describing the scattering of an electron on the molecular cation, and dissociation channels, accounting for atom-atom scattering. The mixing of these channels results in quantum interference of the *direct* mechanism - in which the capture takes place into a doubly excited dissociative state of the neutral system - and the *indirect* one - in which the capture occurs *via* a Rydberg state of the molecule, predissociated by the dissociative state. The direct mechanism dominates the reactive collisions in the cases of favorable crossings (in accordance with the Franck-Condon principle) between the potential energy curves of the dissociative states and that of the target ion. In both mechanisms the autoionization is in competition with the predissociation, and leads to the excitation/de-excitation of the cation. In the present calculations we account for vibrational structure for the target ion's ground electronic state and for the neutral's relevant electronic states, and neglect the rotational effects. A detailed description of our theoretical approach has been given in our previous articles - see for example [20] and [21] and references therein. Here the general ideas and major steps are recalled only. Within a quasi-adiabatic representation of the molecular states, and for a given set of conserved quantum numbers of the neutral system - Λ (projection of the electronic angular momentum on the internuclear axis), S (total electronic spin) - the interaction matrix is built based on the couplings between *ionisation* channels - associated to the vibrational levels v^+ of the cation and to the orbital quantum number l of the incident/Rydberg electron - and *dissociation* channels d_j . By adopting the second-order perturbative solution for the Lippman-Schwinger integral equation [33], we compute the reaction matrix of our collision system in the reaction zone.

A frame transformation is performed eventually, from the Born-Oppenheimer (short range) representation, characterized by v and Λ quantum numbers, valid for small electron-ion and nucleus-nucleus distances, to the close-coupling (long-range) representation, characterized by v^+ , Λ^+ (for the ion) and l (orbital quantum number of the

TABLE I: BeT⁺ vibrational levels relative to the $v_i^+ = 0$. The values of dissociation energies are $D_e = 2.795$ eV and $D_0 = 2.704$ eV.

v_i^+	$E_{v_i^+}$ (eV)	v_i^+	$E_{v_i^+}$ (eV)	v_i^+	$E_{v_i^+}$ (eV)	v_i^+	$E_{v_i^+}$ (eV)
0	0.000	7	1.078	14	1.921	21	2.477
1	0.167	8	1.214	15	2.017	22	2.532
2	0.327	9	1.347	16	2.107	23	2.578
3	0.486	10	1.475	17	2.193	24	2.617
4	0.641	11	1.597	18	2.273	25	2.648
5	0.792	12	1.712	19	2.348	26	2.674
6	0.937	13	1.819	20	2.416	27	2.693

incident/Rydberg electron), valid for both large distances. This frame transformation relies on the quantum defects $\mu_l^\Lambda(R)$ describing the relevant Rydberg series built on the ionic core, and on the eigenvectors and eigenvalues of the K-matrix.

Based on the frame-transformation coefficients, we then build the physical scattering matrix organized in blocks associated to energetically *open* and/or *closed* (O and/or C respectively) channels:

$$S = X_{OO} - X_{OC} \frac{1}{X_{CC} - \exp(-i2\pi\nu)} X_{CO}. \quad (5)$$

The first term in Eq. (5) is restricted to the open channels, resulting in the *direct* mechanism, and the second takes into account their mixing with the closed ones, resulting in the *total*, *i.e.* direct and indirect mechanism, the denominator being responsible for the resonant patterns in the shape of the cross section [17]. Here the matrix $\exp(-i2\pi\nu)$ is diagonal and relies on the effective quantum numbers ν_{v^+} associated to the vibrational thresholds of the closed ionisation channels.

Once we have the scattering matrix the *computation of the cross-sections* is straightforward. For a given target cation on vibrational level v_i^+ and for a given energy of the incident electron ε , the dissociative recombination and the vibrational transition - elastic scattering, excitation, de-excitation - cross sections are computed using, respectively:

$$\sigma_{diss \leftarrow v_i^+} = \frac{\pi}{4\varepsilon} \sum_{l,\Lambda} \rho^\Lambda \sum_j \left| S_{d_j,lv_i^+}^\Lambda \right|^2, \quad (6)$$

$$\sigma_{v_j^+ \leftarrow v_i^+} = \frac{\pi}{4\varepsilon} \sum_{l,l',\Lambda} \rho^\Lambda \left| S_{l'v_j^+,lv_i^+}^\Lambda - \delta_{l'l} \delta_{v_j^+v_i^+} \right|^2. \quad (7)$$

Here ρ^Λ is the ratio between the spin and angular momentum multiplicities of the neutral and the target ion.

III. RESULTS AND DISCUSSIONS

Neglecting the very slight effects related to the change of the nuclear mass when Tritium replace Hydrogen, we have used the molecular data given in Figure 1 of Ref. [20] – namely:

- i) the potential energy curve (PEC) of the ground electronic state of the cation and, for each of the dominant symmetries $^2\Sigma^+$, $^2\Pi$ and $^2\Delta$,
- ii) the PECs of the valence dissociative states of the neutral,
- iii) the quantum defects corresponding to the PECs of the bound Rydberg singly-excited states of the neutral,
- iv) the Rydberg-valence couplings.

Relying on these molecular data, we have performed the inter-nuclear dynamics calculations using the MQDT approach presented in Section II, for the collisions of low-energy electrons with BeT⁺ molecular ions. The DR, VE and VdE cross sections have been calculated for all 28 vibrational levels of the target cation. Table I shows the energies of the vibrational levels of the cation relative to $v_i^+ = 0$ as well as its two spectroscopic dissociation energies (D_e and D_0).

The cross sections have been calculated with the inclusion of both direct and indirect mechanisms for the Σ and Π symmetries, and only the direct mechanism for the Δ symmetry at the highest (*i.e.* second) order of theory. The

cross sections were calculated for each symmetry for the energy range $10^{-5} - 2.7$ eV of the incident electron, having an energy step of 0.01 meV. Thus, we managed to cover the energy range up to the dissociation limit of the ion, i.e. 2.704 eV. The global cross sections - eqs. (6) and (7) - summed up over all symmetries were averaged over a Maxwellian electron energy distribution in order to obtain the thermal rate coefficients up to a maximum electron temperature of 5000 K.

Figures 1–5 show the rate coefficients for DR, VE and VdE of BeT^+ for all the 28 vibrational levels of the electronic ground state. For a given vibrational level of BeT^+ the DR and the VdE rate coefficients have mainly monotonically decreasing tendencies as function of the electron temperature, while the VE ones increase. Moreover, the vibrational dependence of the DR rate coefficients show a monotonically decreasing behavior presenting local maxima for $v_i^+ = 3, 8, 17, 23$ initial target vibrational levels. The DR rate coefficients dominate for $v_i^+ \leq 16$, while for $v_i^+ > 16$ the monovibrational de-excitations become more important.

The excitations are getting important for higher electron temperatures for each vibrational level of the target. For the lower vibrational levels of the BeT^+ cation ($v_i^+ \leq 16$), the VE rates are a notable competitor for DR or the de-excitation processes above 1000 K electron temperature only. For $v_i^+ > 16$, the competition starts at lower temperatures (even below 300 K) and, for the highest vibrational levels ($v_i^+ \geq 24$) and temperatures above 1000 K, VE becomes the dominant process. Notice that the vibrational excitation and de-excitation channels are not necessarily simply connected via detailed balancing, because they involve intermediate states and multi-step processes.

Finally, in order to facilitate kinetic modeling of the beryllium and hydrogen containing plasma and to illustrate the isotopic effect for the beryllium monohydride, we have displayed the rate coefficients for all three isotopologues in the same figure, in two versions.

Figure 6 shows the ratio of the DR rate coefficients for BeD^+ [24] vs BeH^+ [10, 20, 23], and for BeT^+ vs BeH^+ molecular cations, as function of the quantum number of the initial vibrational level of the target and of temperature.

In this representation, the isotopic effect increases with the vibrational quantum number of the target, from very weak for v_i^+ smaller than 5 to very significant for v_i^+ larger than 8, being stronger for BeT^+ than for BeD^+ . This is entirely do to the dependence of the positions of the vibrational levels with respect to the points of crossing between the dissociative PECs and the PEC of the ground state of the target cation.

Figure 7 shows the DR rate coefficients for BeH^+ , BeD^+ and BeT^+ molecular cations as function of the energy of the current vibrational level - relative to the ground ($v_i^+ = 0$) vibrational level (see table I) - for three different electron temperatures, 300, 1000 and 5000 K respectively. Each point or symbol on these curves belongs to a vibrational level of a different isotopologue. The slight shift in each point is due to the slightly different vibrational level spacing induced by the mass difference of the three isotopologues.

Distinct from the common way of plotting such rate coefficients versus vibrational quantum numbers, which in our case leads to a set of three different curves for each considered electron temperature, we now find that the rate coefficients for the three isotopologues versus vibrational energy instead collapse to a very similar (nearly identical) functional form. With the exception of a few points they are essentially the same. This is a very interesting outcome, similar to the one observed already by Capitelli et al [35] for pure neutral hydrogen isotopologues. This similarity law provides scalable rate coefficient functions for all isotopologues with reasonable accuracy starting from rate coefficients calculated for one of them only.

In order to allow the versatile implementation of the rate coefficients shown in figures 1-5 in kinetics modeling codes, unlike our previous studies [10, 24] where we have used generalised Arrhenius formula, here we considered that the original Arrhenius formula is quite suitable for this (cold) plasma application. We also found that this is falling within the range of accuracy provided by quantum chemistry data. As in [30] we will use Arrhenius formula as follows:

$$k^{fitt}(T) = AT^\alpha \exp\left[-\frac{B}{T}\right], \quad (8)$$

for DR and VT (VE and VdE) processes over the electron temperature range $100 \text{ K} \leq T \leq 5000 \text{ K}$. Assuming a Maxwell-Boltzmann vibrational level distribution we have found that vibrational levels up to $v_{max}^+ = 10$ and vibrational transition with $\Delta v_{max} = 10$ are of importance at 5000K electron temperatures. The fitting parameters (A, α, B) are displayed in Tables II–XIII. The numerical values, obtained using the equation (8), agree with the MQDT-computed ones within a range of errors specified in the caption of each table. A maximal relative deviation and an average Root Mean Square (RMS) were provided per data set.

IV. CONCLUSIONS

The present work completes a large series of studies performed on reactive collisions of the beryllium monohydride cation and its isotopologues with low energy electrons, namely for BeH^+ [10, 20, 23], for BeD^+ [24] and for BeT^+ . Making use of the molecular data set calculated in Ref. [20, 22] and by adjusting the nuclear masses, we have performed

an MQDT calculation for all 28 vibrational levels of the heaviest beryllium monohydride cation in collisions with electrons having kinetic energy up to the dissociation limit of the ion.

We have provided rate coefficients for dissociative recombination, vibrational excitation and de-excitation of BeT^+ molecular cation, relevant for detailed kinetic plasma-chemical modeling of the cold edge plasma in fusion devices and for aiding and improving interpretation of spectroscopic beryllium wall release rate experiments. Our present and previously-calculated rate coefficients for the beryllium monohydride isotopologues have been alternatively represented in a comparative way as functions of the target vibrational energy - rather than of the target vibrational quantum number - for different electron temperatures. We found a quite close qualitative and quantitative behavior for all three of these species. This provides a hitherto apparently unexpected similarity scaling law, significantly reducing complexity of the underlying plasma chemical databases for kinetic plasma chemistry models, to be employed in the above mentioned fusion applications. A quite natural but important extension of this finding, left to future work, would be identification (or disproof) of a similar scaling also for the pure hydrogen molecular ions, which is currently already used in fusion boundary codes merely for simplicity, but so far without a posteriori theoretical confirmation.

It is known that beryllium and its compounds are toxic, so no experimental data are provided yet. In this regard, our calculations can be considered as reference. The accuracy of the calculated data is based on our method, which was tested and calibrated with other molecular ions where experimental data can be found. However, we are aware that the main source of error comes from the data obtained from quantum chemistry calculations, which provides us potential energy curves and couplings.

The present article completes the study of *low-energy* collisions of electrons with beryllium monohydride cations. Computations of the high-energy cross sections will start soon, relying on the inclusion of further excited dissociative paths and of the vibrational continuum of the ion, this latter element being at the origin of the dissociative excitation.

Finally we must mention that all the data in tables 1-13 are provided in the Supplementary Materials as ASCII files. Furthermore, the raw data sets of cross sections and rate coefficients are additionally added. Along the way, the data will be uploaded to the LxCat database [36] website.

Acknowledgments

The authors acknowledge support from Fédération de Recherche Fusion par Confinement Magnétique (CNRS, CEA and Eurofusion), La Région Normandie, FEDER and LabEx EMC3 via the projects PTOLEMEE, Bioengine, EMOPlaF, COMUE Normandie Université, the Institute for Energy, Propulsion and Environment (FR-IEPE), the European Union via COST (European Cooperation in Science and Technology) actions TUMIEE (CA17126), MW-Gaia (CA18104) and MD-GAS (CA18212), and ERASMUS-plus conventions between Université Le Havre Normandie and Politehnica University Timisoara, West University Timisoara and University College London. We are indebted to Agence Nationale de la Recherche (ANR) via the project MONA, Centre National de la Recherche Scientifique via the GdR TheMS and the DYMCOM project, and the Institute Pascal, University Paris-Saclay for the warm hospitality during the DYMCOM workshop. NP, FI and JZsM acknowledge support from the UEFISCDI through the mobility project no. PN-III-P1-1.1-MCD-2019-0163. NP is grateful for the support of the Romanian Ministry of Research and Innovation, project no. 10PFE/16.10.2018, PERFORM-TECH-UPT. JZsM thanks the financial support of the National Research, Development and Innovation Fund of Hungary, under the FK 19 funding scheme with project no. FK 132989. The work of DR was carried out under the auspices of the ITER scientists fellow network (ISFN) program, ITER Organization, Route de Vinon-sur-Verdon, CS 90 046 13067 St. Paul-lez-Durance (France).

-
- [1] A.W. Kleyn, N.J. Lopes Cardozo and U. Samm, *Phys. Chem. Chem. Phys.* 8 (2006) 1761.
 - [2] R.E.H Clark and D. Reiter (eds.) *Springer Series in Chemical Physics*, Vol. 78, Springer, Berlin, 2005.
 - [3] R. Celiberto, R.K. Janev and D. Reiter, *Plasma Phys. Control. Fusion* 54 (2012) 035012.
 - [4] O. Motojima, *Nucl. Fusion* 55 (2015) 104023.
 - [5] R. Mitteau, R. Eaton, A. Gervash, V. Kuznetsov, V. Davydov and R. Rulev, *Nuclear Materials and Energy* 12 (2017) 1067.
 - [6] J. Paméla, G.F. Matthews, V. Philipps, R. Kamendje and *JET-EFDA Contributors*, *J. Nucl. Mater.* 363-365 (2007) 1.
 - [7] Borodin *et al*, *Nuclear Materials and Energy*, Volume 9, (2016) 604-609.
 - [8] G. Duxbury, M.F. Stamp and H.P. Summers, *Plasma Phys. Control. Fusion* 40 (1998) 361.
 - [9] D. Darby-Lewis, J. Tennyson, K.D. Lawson, S.N. Yurchenko, M.F. Stamp, A. Shaw, S. Brezinsek and *JET Contributors*, *J. Phys. B: At. Mol. Opt. Phys.* 51 (2018) 185701.
 - [10] S. Niyonzima, S. Ilie, N. Pop, J.Zs. Mezei, K. Chakrabarti, V. Morel, B. Peres, D.A. Little, K. Hassouni, Å. Larson, A.E. Orel, D. Benredjem, A. Bultel, J. Tennyson, D. Reiter and I.F. Schneider, *Atomic Data and Nuclear Data Table* 115-116 (2017) 287.
 - [11] S. Brezinsek *et al*, *Nucl. Fusion* 54 (2014) 103001.
 - [12] S. Brezinsek *et al* and *JET Contributors*, *Nucl. Fusion* 55 (2015) 063021.

- [13] K. Krieger *et al* and *JET-EFDA Contributors*, *J. Nucl. Mater.* 438 (2013) S262.
- [14] D. Nishijima, R.P. Doerner, M.J. Baldwin, G. De Temmerman and E.M. Hollmann, *Plasma Phys. Control. Fusion* 50 (2008) 125007.
- [15] R.P. Doerner, M.J. Baldwin, D. Buchenauer, G. De Temmerman and D. Nishijima, *J. Nucl. Mater.* 390–391 (2009) 681.
- [16] A. Giusti, *J. Phys. B: At. Mol. Phys.* 13 (1980) 3867.
- [17] M.J. Seaton, *Rep. Prog. Phys.* 46 (1983) 16.
- [18] I.F. Schneider, O. Dulieu and A. Giusti-Suzor, *J. Phys. B: At. Mol. Phys.* 24 (1991) L289.
- [19] Ch. Jungen, in: M. Quack and F. Merkt (eds.), *Handbook of High Resolution Spectroscopy*, Wiley, Chichester, New York, 2011, pp. 471–510.
- [20] S. Niyonzima, F. Lique, K. Chakrabarti, Å. Larson, A.E. Orel and I.F. Schneider, *Phys. Rev A* 87 (2013) 022713.
- [21] J.Zs. Mezei, K. Chakrabarti, M.D. Epée Epée, O. Motapon, Ch.H. Yuen, M.A. Ayouz, N. Douguet, S. Fonseca dos Santos, V. Kokoouline and I.F. Schneider, *ACS Earth Space Chem.* 3 (2019) 2376.
- [22] J.B. Roos, M. Larsson, Å. Larson and A.E. Orel, *Phys. Rev. A* 80 (2009) 012501.
- [23] V. Laporta, K. Chakrabarti, R. Celiberto, R.K. Janev, J.Zs. Mezei, S. Niyonzima, J. Tennyson and I.F. Schneider, *Plasma Physics and Control. Fusion* 59 (2017) 045008.
- [24] S. Niyonzima, N. Pop, F. Iacob, Å. Larson, A.E. Orel, J.Zs. Mezei, K. Chakrabarti, V. Laporta, K. Hassouni, D. Benredjem, A. Bultel, J. Tennyson, D. Reiter and I.F. Schneider, *Plasma Sources Sci. Technol.* 27 (2018) 025015.
- [25] F. Iacob, N. Pop, J.Zs. Mezei, M.D. Epée Epée, O. Motapon, S. Niyonzima, V. Laporta and I.F. Schneider, *AIP Conference Proceedings* 2071 (2019) 020007.
- [26] N. Pop, F. Iacob, J. Z. Mezei, O. Motapon, S. Niyonzima, D. Kashinski, D. Talbi, A. P. Hickman and I. F. Schneider, *AIP Conference Proceedings* 1916 (2017) 020013
- [27] R.A. Pitts *et al.*, 2019 *Nucl. Mat. and Energy* 20 (2019) 100696.
- [28] Felix Iacob, *Physics Letters A*, 384, 35, (2020), 126888,
- [29] O. Motapon, N. Pop, F. Argoubi, J.Zs. Mezei, M.D. Epée Epée, A. Faure, M. Telmini, J. Tennyson and I.F. Schneider, *Phys. Rev. A* 90 (2014) 012706.
- [30] D. A. Little, K. Chakrabarti, J.Zs. Mezei, I.F. Schneider and J. Tennyson, *Phys. Rev. A* 90 (2014) 052705.
- [31] Y. Moulane, J.Zs. Mezei, V. Laporta, E. Jehin, Z. Benkhaldoun and I.F. Schneider, *A&A* 613 (2018) A53.
- [32] V. Kokoouline, M.A. Ayouz, J.Zs. Mezei, K. Hassouni and I.F. Schneider, *Plasma Sources Sci. Technol.* 27 (2018) 115007.
- [33] V. Ngassam, A. Florescu, L. Pichl, I.F. Schneider, O. Motapon and A. Suzor-Weiner, *Eur. Phys. J. D* 26 (2003) 165.
- [34] M.A. Ayouz, Ch.H. Yuen, N. Balucani, C. Ceccarelli, I.F. Schneider and V. Kokoouline, *Mon. Not. R. Astron. Soc.* 490 (2019) 1325.
- [35] M. Capitelli *et al*, *Nucl. Fusion* 46 (2006) S260.
- [36] S. Pancheshnyi, S. Biagi, M. C. Bordage, G. J. M. Hagelaar, W. L. Morgan, A. V. Phelps, L. C. Pitchford, *Chem. Phys.* 398 (2012) 148.

Appendix

Explanation of figures:

Figures 1-5. Dissociative recombination, vibrational excitation and de-excitation Maxwell rate coefficients for all the vibrational levels of BeH^+ in its ground electronic state.

Ordinate	Maxwell rate coefficient in $\text{cm}^3 \cdot \text{s}^{-1}$
Abscissa	Electron temperature in K
Thick black line	DR Maxwell rate coefficient
Thin coloured lines	Vibrational excitation rate coefficients
Coloured lines with symbols	Vibrational de-excitation rate coefficients

Figure 6. Ratios of the dissociative recombination rate coefficients for BeD^+ *vs* BeH^+ (left), and for BeT^+ *vs* BeH^+ (right) molecular cations, as function of the quantum number of the initial vibrational level of the target and of temperature.

Ordinate	Ratios of dissociative recombination Maxwell rate coefficients
Abscissa	Electron temperature in K

Figure 7. Dissociative recombination rate coefficient for the three beryllium monohydride isotopologues cations as function of the energy of the initial vibrational level of the target - relative to the ground vibrational level - for three different electron temperatures.

Ordinate	Dissociative recombination Maxwell rate coefficient in $\text{cm}^3 \cdot \text{s}^{-1}$
Abscissa	Vibrational energy relative to the ground level in eV.
Black curves	DR rate coefficients for BeH^+ .
Blue curves	DR rate coefficients for BeD^+ .
Red curves	DR rate coefficients for BeT^+ .
Dashed coloured curves with symbols	DR rate coefficients at $T = 300$ K electron temperature.
Continuous coloured curves with symbols	DR rate coefficients at $T = 1000$ K electron temperature.
Dashed-dotted coloured curves with symbols	DR rate coefficients at $T = 5000$ K electron temperature.

In order to facilitate the use of the rate coefficients given in figure 7 we have presented them in tables XIV and XV. The data obtained for each of the three isotopologues are suitable to represent the behavior as a function of the vibrational energy.

Explanation of tables:

Table II. List of fitting parameters according to eq. (8), minimum and maximum values of relative difference and root mean squares calculated for dissociative recombination for the $v_i^+ = 0 - 10$ vibrational levels of the ground electronic state of BeT^+ .

v_i^+	Initial vibrational level of BeT^+
Temperature range	in K
A, α, B	Fitting parameters
$\text{rd}_{max} = \max_{i=1, \dots, n} \left \frac{k_i(T) - k_i^{fitt}(T)}{k_i(T)} \right $	maximum of relative difference
$\text{RMS} = \sqrt{\sum_{i=1}^n \frac{1}{n} \left \frac{k_i(T) - k_i^{fitt}(T)}{k_i(T)} \right ^2}$	root mean square

Tables III–XIII. List of fitting parameters according to eq. (8), minimum and maximum values of relative difference and root mean squares calculated for vibrational transitions ($\Delta v_{max} = 10$) for the $v_i^+ = 0 - 10$ vibrational levels of the ground electronic state of BeT^+ .

$v_i^+ \rightarrow v_f^+$	Vibrational transition of BeT^+
$v_i^+ \rightarrow v_f^+$	Stands for VdE
Temperature range	in K
A, α, B	Fitting parameters
$\text{rd}_{max} = \max_{i=1, \dots, n} \left \frac{k_i(T) - k_i^{fitt}(T)}{k_i(T)} \right $	maximum of relative difference
$\text{RMS} = \sqrt{\sum_{i=1}^n \frac{1}{n} \left \frac{k_i(T) - k_i^{fitt}(T)}{k_i(T)} \right ^2}$	root mean square

Note: In Tables II–XIII the coefficients were given taking into account a wider temperature range in order to prevent boundary errors. The temperature range was increased with 10% of the boundary values. The global maximal value of relative difference was taken as the maximum among all DR maximum relative differences and the maximum among all VT values for a given target. The average RMS was calculated as the arithmetic mean of the temperature weighted process RMS values.

Tables XIV–XV. List of dissociative recombination rate coefficient showing the isotopic effects displayed in figure 7.

Temperature range	in K
v_i^+	Initial vibrational level of BeX^+
$E_{v_i^+} - E_0$	Energy difference relative to the ground state
Rate coefficient	in (cm^3/s)
Data by columns corresponding to $\text{BeX}^+ \in \{\text{BeH}^+, \text{BeD}^+, \text{BeT}^+\}$ isotopologues	

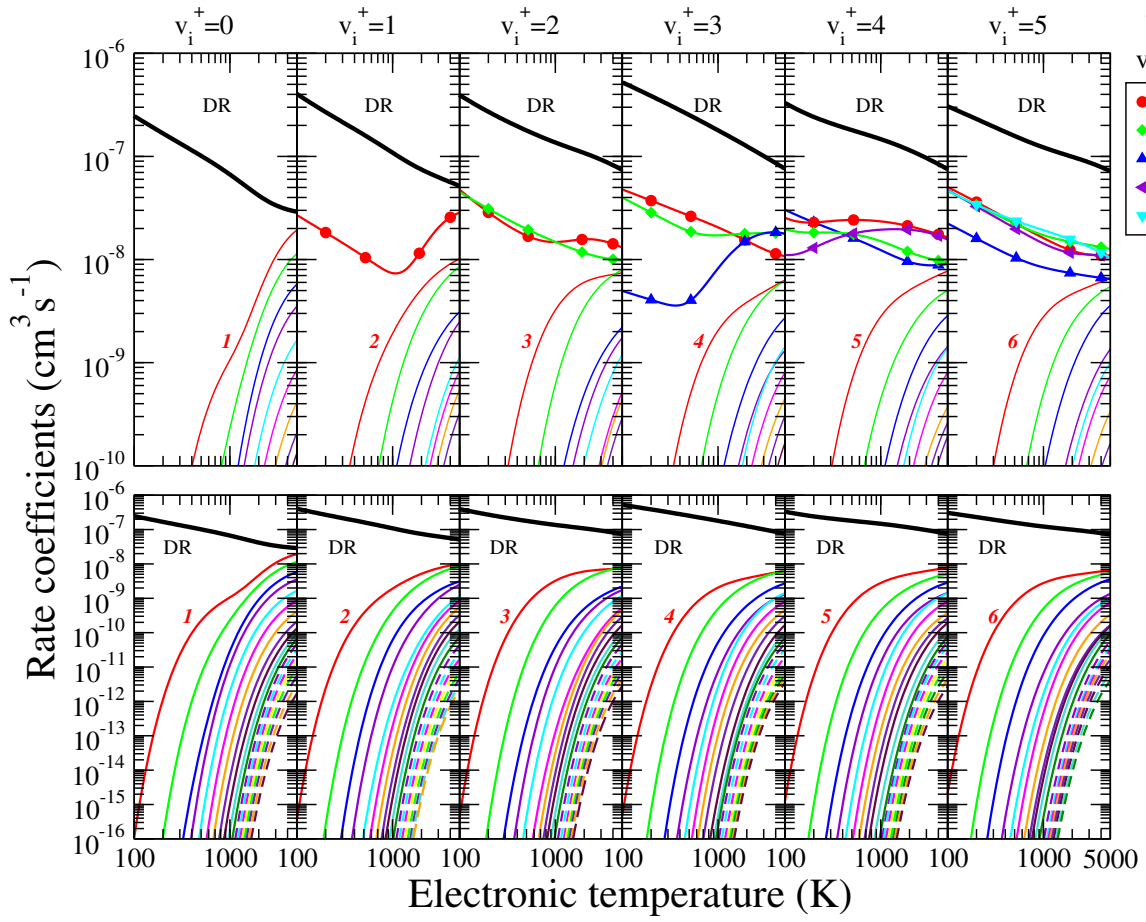


FIG. 1: Dissociative recombination (DR, thick black line), vibrational excitation (VE, thin coloured solid and dashed lines) and vibrational de-excitation (VdE, symbols and thick coloured lines) rate coefficients of BeT⁺ in its electronic ground state and for the initial vibrational levels $v_i^+ = 0 - 5$. Upper panels: for each v_i^+ of BeT⁺, all possible de-excitation final vibrational quantum numbers are given, while for the excitation only the first one is labeled. The VE rate coefficients decreases monotonically with the increase of the final vibrational quantum numbers of the target ion. Lower panels: DR and VE rate coefficients only, with the panels extended down to $10^{-16} \text{ cm}^3 \cdot \text{s}^{-1}$.

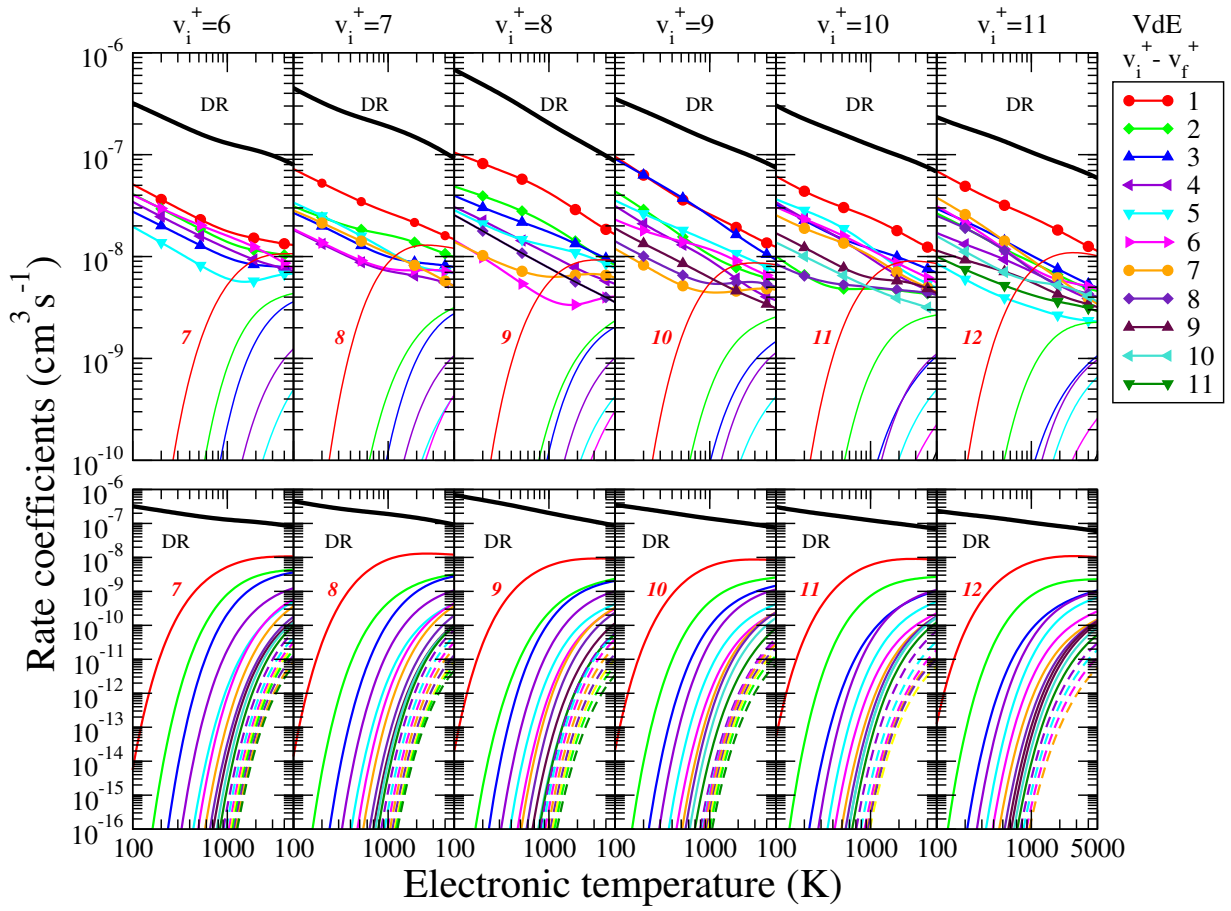


FIG. 2: Same as in figure 1 for $v_i^+ = 6 - 11$.

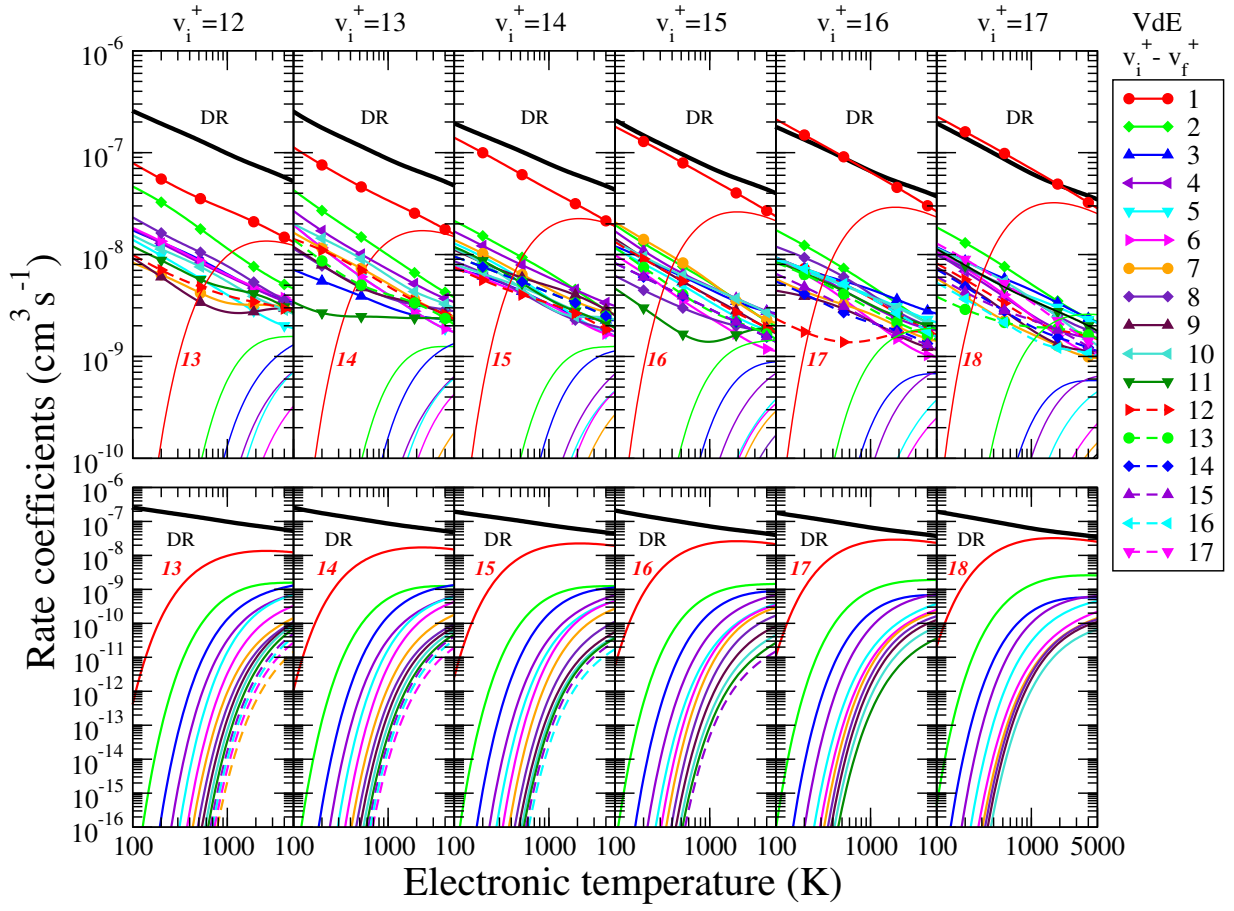


FIG. 3: Same as in figure 1 for $v_i^+ = 12 - 17$.

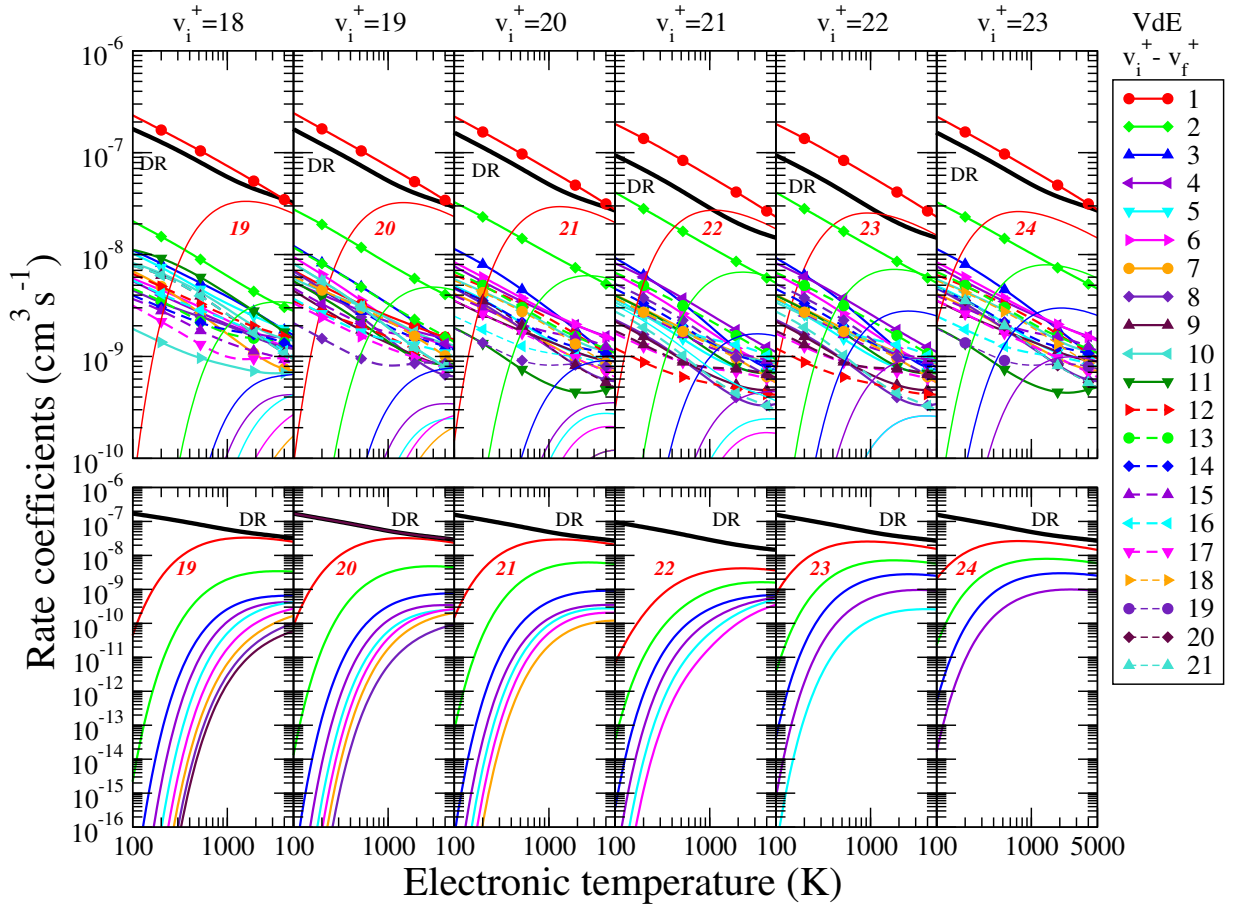


FIG. 4: Same as in figure 1 for $v_i^+ = 18 - 23$.

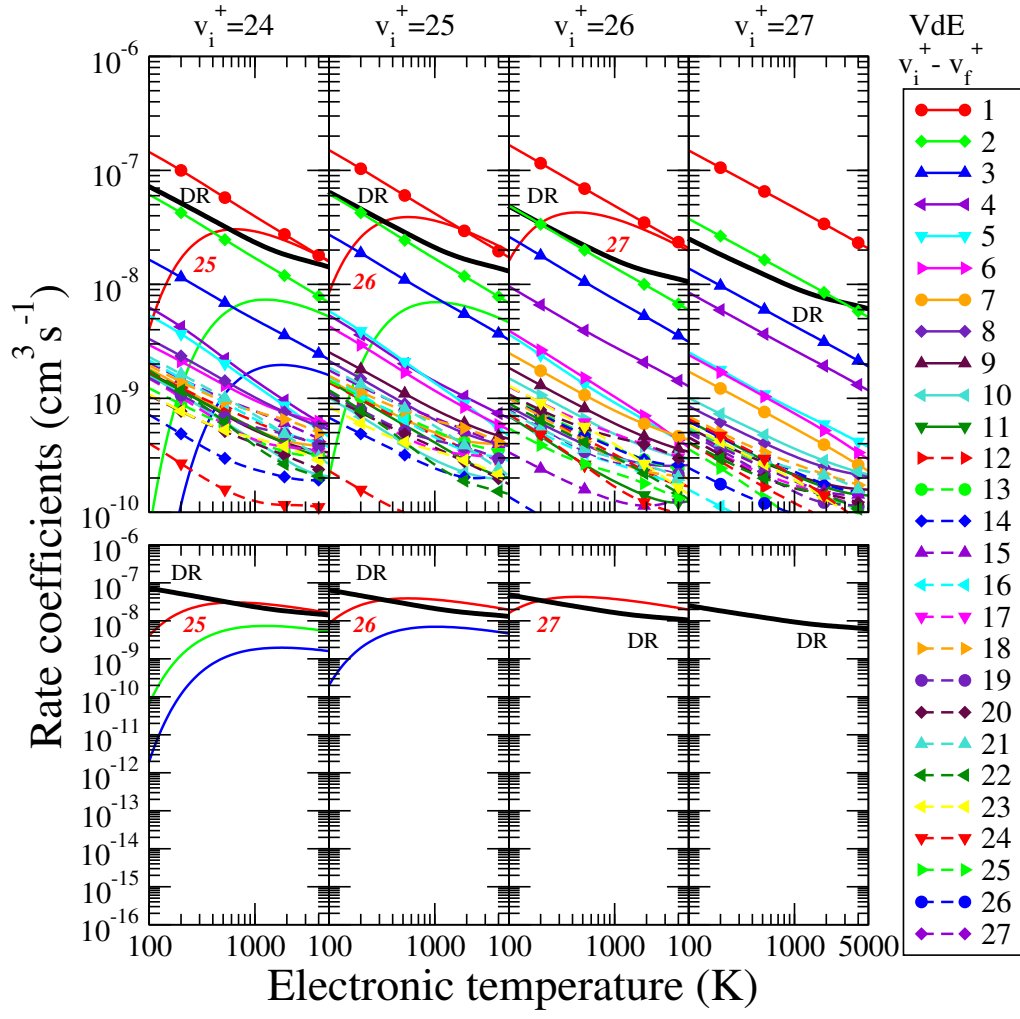


FIG. 5: Same as in figure 1 for $v_i^+ = 24 - 27$.

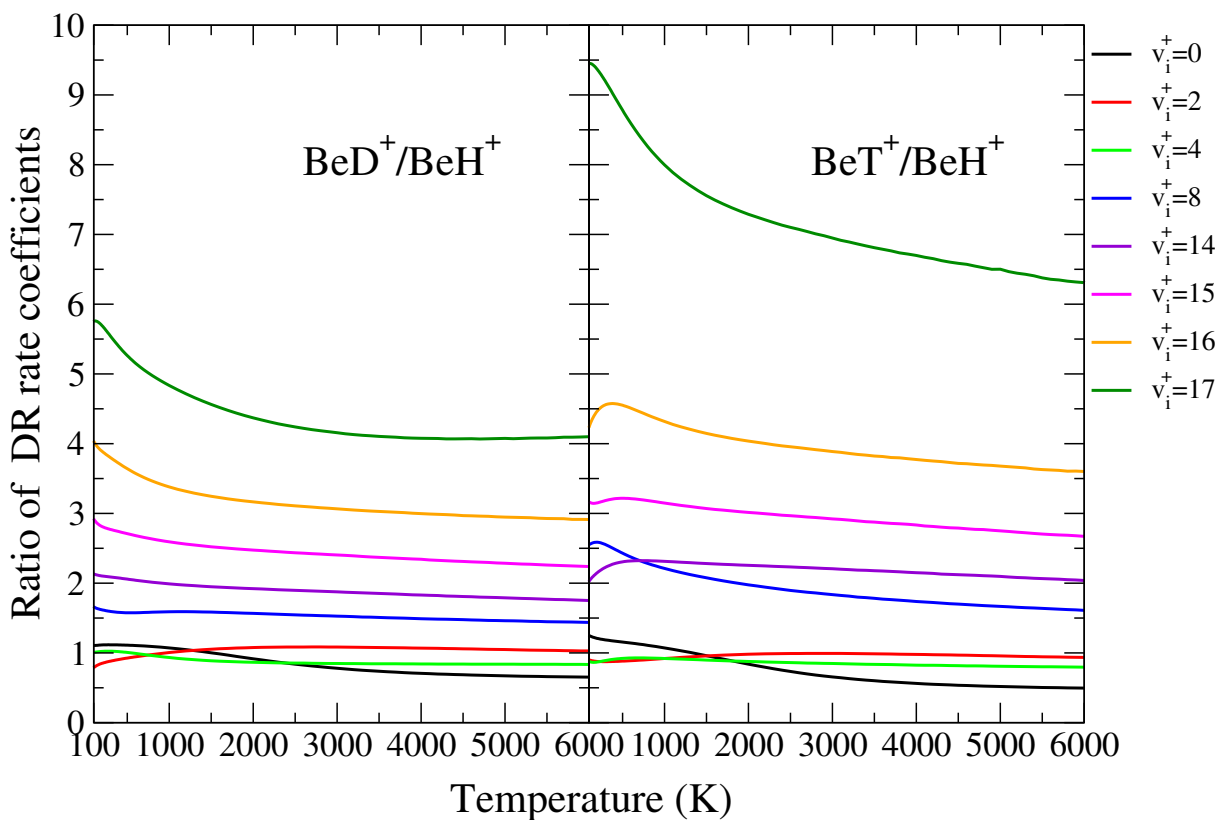


FIG. 6: Isotopic effects: Ratios of the dissociative recombination rate coefficients for BeD^+ [24] *vs* BeH^+ [10, 20, 23] (left), and for BeT^+ *vs* BeH^+ (right) molecular cations, as function of the quantum number of the initial vibrational level of the target and of temperature.

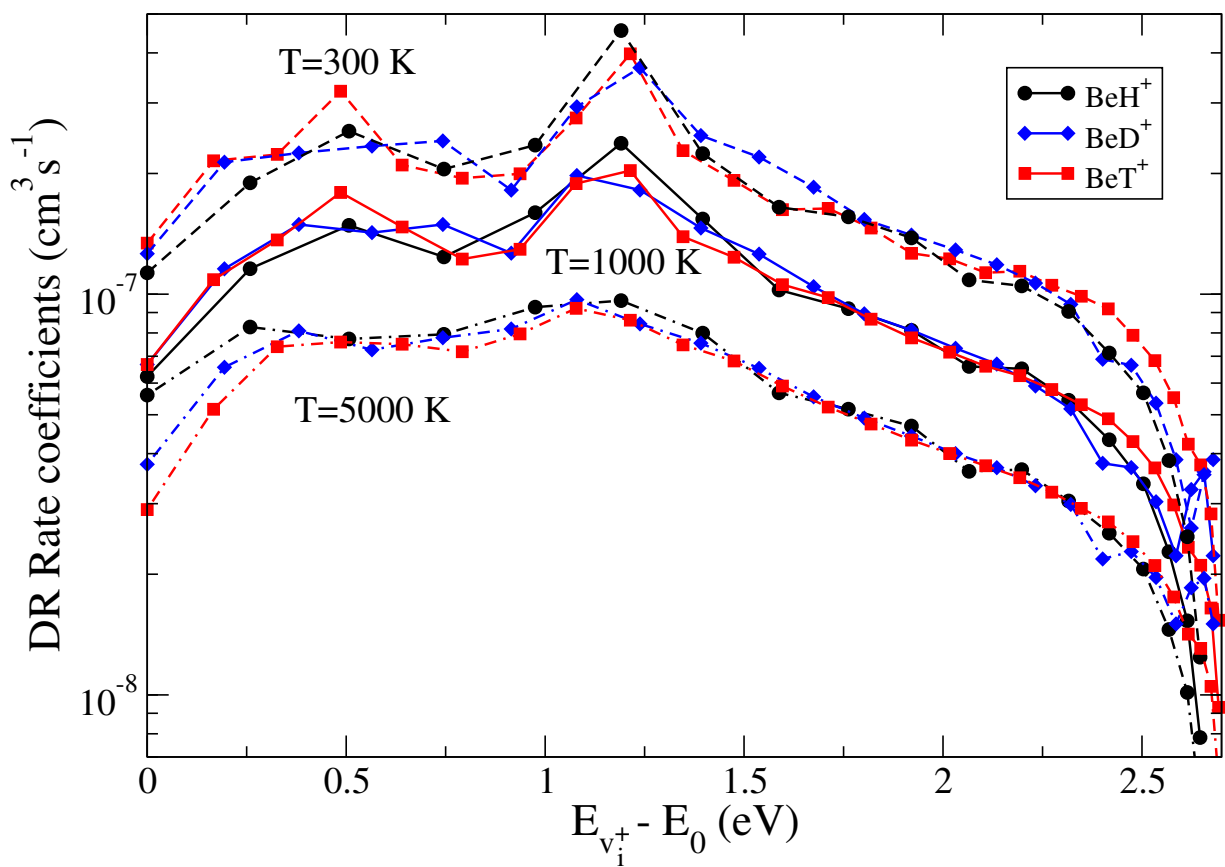


FIG. 7: Isotopic effects: Dissociative recombination rate coefficient of the BeH^+ (black curves with circles), BeD^+ (blue curves with diamonds) and BeT^+ (red curves with squares) molecular cations as function of the energy of the initial vibrational level of the target - relative to the ground vibrational level - for three electron temperatures.

TABLE II: Fitting parameters for the DR Maxwell rate coefficients of $\text{BeT}^+(v_i^+ = 0, \dots, 10)$, for temperatures ranging between 100 K and 5000 K as displayed in figures 1–5. The calculated rate coefficients are reproduced with a maximal relative deviation of 3.242% and with an average Root Mean Square (RMS) of 0.0064.

v_i^+	Temperature range (K)	A (cm^3/s)	α	B (K)
0	$100 \leq T \leq 1000$	$3.28197 \cdot 10^{-6}$	-0.560182	1.28522
	$1000 < T \leq 5000$	$1.2742 \cdot 10^{-7}$	-0.193793	-715.096
1	$100 \leq T \leq 1500$	$4.93965 \cdot 10^{-6}$	-0.551551	-3.05762
	$1500 < T \leq 5000$	$5.54357 \cdot 10^{-7}$	-0.286297	-345.175
2	$100 \leq T \leq 1500$	$1.59139 \cdot 10^{-6}$	-0.359808	-26.6809
	$1500 < T \leq 5000$	$8.88933 \cdot 10^{-6}$	-0.551753	429.823
3	$100 \leq T \leq 5000$	$6.41436 \cdot 10^{-6}$	-0.517293	13.1328
4	$100 \leq T \leq 1000$	$6.98686 \cdot 10^{-7}$	-0.228439	-30.1691
	$1000 < T \leq 5000$	$8.75990 \cdot 10^{-6}$	-0.551726	279.519
5	$100 \leq T \leq 1000$	$1.81880 \cdot 10^{-6}$	-0.393492	-3.40054
	$1000 < T \leq 5000$	$2.01551 \cdot 10^{-6}$	-0.386694	140.669
6	$100 \leq T \leq 5000$	$8.97394 \cdot 10^{-7}$	-0.281268	-28.9724
7	$100 \leq T \leq 1000$	$1.08752 \cdot 10^{-6}$	-0.258424	-31.4290
	$100 \leq T \leq 5000$	$1.82852 \cdot 10^{-5}$	-0.612179	350.171
8	$100 \leq T \leq 1000$	$8.0781 \cdot 10^{-6}$	-0.539215	0.11067
	$1000 < T \leq 5000$	$1.0082 \cdot 10^{-5}$	-0.561074	11.15700
9	$100 \leq T \leq 1000$	$1.7769 \cdot 10^{-6}$	-0.360498	-3.68476
	$1000 < T \leq 5000$	$2.0542 \cdot 10^{-6}$	-0.388174	-3.37710
10	$100 \leq T \leq 1000$	$2.7190 \cdot 10^{-6}$	-0.467593	-0.13565
	$1000 \leq T \leq 5000$	$2.6040 \cdot 10^{-6}$	-0.423590	128.7260

TABLE III: Fitting parameters for the VT ($\Delta v_{max} = 10$) Maxwell rate coefficients of $\text{BeT}^+(v_i^+ = 0)$, for temperatures ranging between 100 K and 5000 K, as displayed in figure 1. The calculated rate coefficients are reproduced with a maximal relative deviation of 6.073% and with an average RMS of 0.0108.

$v_i^+ \rightarrow v_f^+$	Temperature range (K)	A (cm^3/s)	α	B (K)
$0 \rightarrow 1$	$100 \leq T \leq 800$	$5.55127 \cdot 10^{-7}$	-0.631862	1946.6
	$800 < T \leq 1700$	$6.82095 \cdot 10^{-20}$	3.19051	-1420.11
	$1700 < T \leq 5000$	$2.18465 \cdot 10^{-6}$	-0.41325	6020.8
$0 \rightarrow 2$	$200 \leq T \leq 540$	$5.61 \cdot 10^{-8}$	-0.277382	3703.32
	$540 < T \leq 1700$	$1.69648 \cdot 10^{-14}$	1.71428	2320.49
	$1700 < T \leq 5000$	$1.8088 \cdot 10^{-6}$	-0.439072	6608.15
$0 \rightarrow 3$	$320 \leq T \leq 700$	$1.96702 \cdot 10^{-16}$	2.42111	4758.72
	$700 < T \leq 1500$	$4.0198 \cdot 10^{-9}$	0.242131	6595.09
	$1500 < T \leq 5000$	$1.94918 \cdot 10^{-5}$	-0.755523	8455.75
$0 \rightarrow 4$	$400 \leq T \leq 1500$	$7.19563 \cdot 10^{-8}$	-0.156832	7658.54
	$1500 < T \leq 5000$	$7.81868 \cdot 10^{-6}$	-0.696791	8849.87
$0 \rightarrow 5$	$460 \leq T \leq 1500$	$2.62787 \cdot 10^{-7}$	-0.367603	9262.82
	$1500 < T \leq 5000$	$5.20392 \cdot 10^{-6}$	-0.710329	10044.6
$0 \rightarrow 6$	$560 \leq T \leq 1500$	$5.36862 \cdot 10^{-7}$	-0.486471	11014.8
	$1500 < T \leq 5000$	$8.72782 \cdot 10^{-6}$	-0.808104	11756.5
$0 \rightarrow 7$	$650 \leq T \leq 1500$	$2.72072 \cdot 10^{-7}$	-0.460102	12561.0
	$1500 < T \leq 5000$	$3.60645 \cdot 10^{-6}$	-0.753226	13304.5
$0 \rightarrow 8$	$750 \leq T \leq 1500$	$2.22274 \cdot 10^{-7}$	-0.487693	14077.8
	$1500 < T \leq 5000$	$1.37401 \cdot 10^{-6}$	-0.685974	14745.6
$0 \rightarrow 9$	$850 \leq T \leq 1700$	$7.47373 \cdot 10^{-8}$	-0.37838	15497.4
	$1700 < T \leq 5000$	$1.16235 \cdot 10^{-6}$	-0.678763	16486.9
$0 \rightarrow 10$	$950 \leq T \leq 2000$	$1.76168 \cdot 10^{-8}$	-0.212531	16919.9
	$2000 < T \leq 5000$	$2.31428 \cdot 10^{-6}$	-0.755505	18522.3

TABLE IV: Same as table III for $v_i^+ = 1$, as displayed in figure 1, maximal relative deviation of 6.459% and average RMS of 0.0098.

$v_i^+ \rightarrow v_f^+$	Temperature range (K)	A (cm^3/s)	α	B (K)
1 \rightarrow 0	$100 \leq T \leq 1000$	$4.50249 \cdot 10^{-7}$	-0.599873	5.30000
	$1000 < T \leq 2500$	$2.43483 \cdot 10^{-16}$	2.21315	-1823.33
	$2500 < T \leq 5000$	$1.8544 \cdot 10^{-5}$	-0.643767	4975.26
1 \rightarrow 2	$100 \leq T \leq 300$	$2.55835 \cdot 10^{-7}$	-0.467812	1818.6
	$300 < T \leq 900$	$4.45218 \cdot 10^{-9}$	0.102817	1562.25
	$900 < T \leq 5000$	$5.70154 \cdot 10^{-9}$	0.112954	1901.61
1 \rightarrow 3	$190 \leq T \leq 400$	$7.33653 \cdot 10^{-8}$	-0.243628	3630.72
	$400 < T \leq 1300$	$3.59106 \cdot 10^{-9}$	0.303087	3419.43
	$1300 < T \leq 5000$	$4.92087 \cdot 10^{-8}$	-0.110554	4050.88
1 \rightarrow 4	$280 \leq T \leq 1500$	$6.03362 \cdot 10^{-7}$	-0.507352	5686.01
	$1500 < T \leq 5000$	$1.92775 \cdot 10^{-8}$	-0.096070	5036.37
1 \rightarrow 5	$360 \leq T \leq 1000$	$9.45769 \cdot 10^{-8}$	-0.295715	7099.65
	$1000 < T \leq 2500$	$9.96048 \cdot 10^{-10}$	0.267671	6422.72
	$2500 < T \leq 5000$	$2.40339 \cdot 10^{-7}$	-0.344658	8178.08
1 \rightarrow 6	$480 \leq T \leq 1000$	$1.60089 \cdot 10^{-9}$	-0.127208	8485.23
	$1000 < T \leq 2500$	$2.88654 \cdot 10^{-11}$	0.636106	8003.94
	$2500 < T \leq 5000$	$2.48387 \cdot 10^{-7}$	-0.378268	10844.1
1 \rightarrow 7	$560 \leq T \leq 1700$	$1.02492 \cdot 10^{-9}$	0.234332	10195.0
	$1700 < T \leq 5000$	$8.8946 \cdot 10^{-7}$	-0.535633	12076.0
1 \rightarrow 8	$650 \leq T \leq 1700$	$7.23629 \cdot 10^{-10}$	0.273121	11880.6
	$1700 < T \leq 5000$	$3.37484 \cdot 10^{-6}$	-0.692863	14159.8
1 \rightarrow 9	$750 \leq T \leq 1800$	$8.58581 \cdot 10^{-10}$	0.230284	13453.3
	$1800 < T \leq 5000$	$7.40756 \cdot 10^{-6}$	-0.804795	15920.4
1 \rightarrow 10	$800 \leq T \leq 1700$	$7.91052 \cdot 10^{-9}$	-0.045485	15121.1
	$1700 < T \leq 5000$	$2.45025 \cdot 10^{-5}$	-0.965532	17280.1
1 \rightarrow 11	$900 \leq T \leq 1800$	$5.55123 \cdot 10^{-8}$	-0.295216	16841.5
	$1800 < T \leq 5000$	$5.33313 \cdot 10^{-5}$	-1.0799	18708.8

TABLE V: Same as table III for $v_i^+ = 2$, as displayed in figure 1, maximal relative deviation of 5.369% and average RMS of 0.0079.

$v_i^+ \rightarrow v_f^+$	Temperature range (K)	A (cm^3/s)	α	B (K)
2 \rightarrow 1	$100 \leq T \leq 650$	$1.98340 \cdot 10^{-7}$	-0.410144	-47.2313
	$650 < T \leq 2500$	$2.67382 \cdot 10^{-9}$	0.217131	-221.517
	$2500 < T \leq 5000$	$1.03204 \cdot 10^{-5}$	-0.743861	1679.41
2 \rightarrow 0	$100 \leq T \leq 1000$	$2.65852 \cdot 10^{-7}$	-0.422904	-18.0281
	$1000 < T \leq 5000$	$1.41619 \cdot 10^{-8}$	-0.055055	-438.763
2 \rightarrow 3	$100 \leq T \leq 750$	$2.98556 \cdot 10^{-7}$	-0.385583	1857.56
	$750 < T \leq 5000$	$1.52063 \cdot 10^{-7}$	-0.317954	1649.34
2 \rightarrow 4	$180 \leq T \leq 460$	$5.39078 \cdot 10^{-8}$	-0.108704	3706.07
	$460 < T \leq 1500$	$1.79330 \cdot 10^{-7}$	-0.270308	3810.89
	$1500 < T \leq 5000$	$4.21512 \cdot 10^{-7}$	-0.373900	3955.53
2 \rightarrow 5	$280 \leq T \leq 750$	$1.47486 \cdot 10^{-8}$	-0.104801	5239.98
	$750 < T \leq 5000$	$1.07730 \cdot 10^{-8}$	-0.064429	5185.79
2 \rightarrow 6	$360 \leq T \leq 950$	$1.63766 \cdot 10^{-7}$	-0.383215	7049.35
	$950 < T \leq 5000$	$4.35176 \cdot 10^{-8}$	-0.214698	6932.32
2 \rightarrow 7	$460 \leq T \leq 1000$	$5.07710 \cdot 10^{-7}$	-0.548890	8732.22
	$1000 < T \leq 2500$	$2.29574 \cdot 10^{-9}$	0.108113	7824.24
	$2500 < T \leq 5000$	$3.27557 \cdot 10^{-8}$	-0.181104	8832.80
2 \rightarrow 8	$560 \leq T \leq 1200$	$3.04328 \cdot 10^{-10}$	0.265882	9619.67
	$1200 < T \leq 2500$	$4.32959 \cdot 10^{-12}$	0.789060	8969.37
	$2500 < T \leq 5000$	$7.05150 \cdot 10^{-8}$	-0.293284	12085.2
2 \rightarrow 9	$650 \leq T \leq 1900$	$4.62304 \cdot 10^{-10}$	0.282399	11528.0
	$1900 < T \leq 5000$	$5.15463 \cdot 10^{-7}$	-0.509966	13597.4
2 \rightarrow 10	$750 \leq T \leq 2000$	$6.43134 \cdot 10^{-9}$	-0.046700	13239.8
	$2000 < T \leq 5000$	$3.16506 \cdot 10^{-7}$	-0.479755	14524.7
2 \rightarrow 11	$800 \leq T \leq 1900$	$3.04332 \cdot 10^{-8}$	-0.276149	14504.1
	$1900 < T \leq 5000$	$9.65857 \cdot 10^{-8}$	-0.392462	15116.6
2 \rightarrow 12	$850 \leq T \leq 2000$	$3.35235 \cdot 10^{-8}$	-0.308151	15744.6
	$2000 < T \leq 5000$	$3.55228 \cdot 10^{-7}$	-0.565695	16623.0

TABLE VI: Same as table III for $v_i^+ = 3$, as displayed in figure 1, maximal relative deviation of 4.869% and average RMS of 0.0064.

$v_i^+ \rightarrow v_f^+$	Temperature range (K)	A (cm^3/s)	α	B (K)
3 \rightarrow 2	$100 \leq T \leq 5000$	$3.46715 \cdot 10^{-7}$	-0.410553	9.90469
3 \rightarrow 1	$100 \leq T \leq 650$	$2.12157 \cdot 10^{-7}$	-0.394035	-15.1628
	$650 < T \leq 5000$	$1.58371 \cdot 10^{-8}$	0.015527	18.2980
3 \rightarrow 0	$100 \leq T \leq 380$	$8.75244 \cdot 10^{-9}$	-0.163227	-19.2090
	$380 < T \leq 1000$	$1.36004 \cdot 10^{-15}$	2.15314	-751.922
	$1000 < T \leq 5000$	$2.54536 \cdot 10^{-6}$	-0.531187	2127.30
3 \rightarrow 4	$100 \leq T \leq 400$	$1.73997 \cdot 10^{-7}$	-0.378735	1800.43
	$400 < T \leq 1500$	$2.53625 \cdot 10^{-7}$	-0.435000	1813.83
	$1500 < T \leq 5000$	$2.33805 \cdot 10^{-10}$	0.397347	443.964
3 \rightarrow 5	$180 \leq T \leq 540$	$1.91749 \cdot 10^{-7}$	-0.357808	3511.67
	$540 < T \leq 1500$	$1.85672 \cdot 10^{-8}$	-0.046832	3300.15
	$1500 < T \leq 5000$	$7.81031 \cdot 10^{-8}$	-0.210848	3672.47
3 \rightarrow 6	$270 \leq T \leq 750$	$8.51869 \cdot 10^{-8}$	-0.324917	5161.45
	$750 < T \leq 2000$	$2.54974 \cdot 10^{-9}$	0.122469	4737.41
	$2000 < T \leq 5000$	$2.16745 \cdot 10^{-8}$	-0.117307	5390.10
3 \rightarrow 7	$360 \leq T \leq 1000$	$4.41787 \cdot 10^{-9}$	0.036043	6626.28
	$1000 < T \leq 2500$	$5.03471 \cdot 10^{-8}$	-0.258383	7048.81
	$2500 < T \leq 5000$	$3.83663 \cdot 10^{-7}$	-0.487105	7658.27
3 \rightarrow 8	$440 \leq T \leq 1200$	$5.57754 \cdot 10^{-8}$	-0.212691	8466.71
	$1200 < T \leq 5000$	$1.46301 \cdot 10^{-6}$	-0.599417	9162.28
3 \rightarrow 9	$520 \leq T \leq 1500$	$1.24894 \cdot 10^{-6}$	-0.630400	10297.4
	$1500 < T \leq 5000$	$3.04057 \cdot 10^{-7}$	-0.460993	10053.8
3 \rightarrow 10	$650 \leq T \leq 1500$	$1.48874 \cdot 10^{-6}$	-0.698783	11634.5
	$1500 < T \leq 5000$	$1.54147 \cdot 10^{-7}$	-0.417352	11387.4
3 \rightarrow 11	$700 \leq T \leq 1200$	$8.17357 \cdot 10^{-8}$	-0.385387	12622.1
	$1200 < T \leq 2500$	$1.27242 \cdot 10^{-9}$	0.121714	11933.6
	$2500 < T \leq 5000$	$4.55953 \cdot 10^{-7}$	-0.532978	13861.3
3 \rightarrow 12	$800 \leq T \leq 2000$	$8.98344 \cdot 10^{-11}$	0.416906	13704.7
	$2000 < T \leq 5000$	$9.46224 \cdot 10^{-7}$	-0.628390	16455.0
3 \rightarrow 13	$900 \leq T \leq 2500$	$2.32460 \cdot 10^{-9}$	0.002630	15463.8
	$2500 < T \leq 5000$	$5.98830 \cdot 10^{-7}$	-0.614689	17301.9

TABLE VII: Same as table III for $v_i^+ = 4$, as displayed in figure 1, maximal relative deviation of 6.067% and average RMS of 0.0047.

$v_i^+ \rightarrow v_f^+$	Temperature range (K)	A (cm^3/s)	α	B (K)
4 \rightarrow 3	$100 \leq T \leq 200$	$1.06736 \cdot 10^{-9}$	0.494538	-89.1826
	$200 < T \leq 700$	$3.68736 \cdot 10^{-8}$	-0.056086	37.2856
	$700 < T \leq 5000$	$3.40362 \cdot 10^{-7}$	-0.349760	255.420
4 \rightarrow 2	$100 \leq T \leq 400$	$9.47838 \cdot 10^{-9}$	0.0986899	-26.4064
	$400 < T \leq 1000$	$4.68070 \cdot 10^{-7}$	-0.4725691	170.016
	$1000 < T \leq 5000$	$3.33750 \cdot 10^{-8}$	-0.157519	-307.015
4 \rightarrow 1	$100 \leq T \leq 1000$	$1.59446 \cdot 10^{-7}$	-0.368440	-3.36955
	$1000 < T \leq 2500$	$1.29462 \cdot 10^{-8}$	-0.069683	-437.410
	$2500 < T \leq 5000$	$1.38102 \cdot 10^{-10}$	0.455216	-1536.81
4 \rightarrow 0	$100 \leq T \leq 400$	$7.22006 \cdot 10^{-10}$	0.514608	-32.8827
	$400 < T \leq 1000$	$8.18946 \cdot 10^{-7}$	-0.447542	666.741
	$1000 < T \leq 5000$	$2.46285 \cdot 10^{-10}$	0.391802	-1330.58
4 \rightarrow 5	$120 \leq T \leq 400$	$5.49606 \cdot 10^{-7}$	-0.512713	1754.28
	$400 < T \leq 800$	$3.72401 \cdot 10^{-7}$	-0.457827	1729.88
	$800 < T \leq 5000$	$2.82849 \cdot 10^{-7}$	0.139895	973.706
4 \rightarrow 6	$240 \leq T \leq 500$	$3.76215 \cdot 10^{-7}$	-0.480352	3439.51
	$500 < T \leq 1700$	$1.23983 \cdot 10^{-8}$	-0.003322	3097.05
	$1700 < T \leq 5000$	$4.55290 \cdot 10^{-8}$	-0.176574	3510.89
4 \rightarrow 7	$240 \leq T \leq 650$	$7.06310 \cdot 10^{-8}$	-0.297187	4995.04
	$650 < T \leq 2000$	$4.11467 \cdot 10^{-9}$	0.075303	4708.91
	$2000 < T \leq 5000$	$6.05544 \cdot 10^{-8}$	-0.230307	5456.78
4 \rightarrow 8	$360 \leq T \leq 1000$	$3.44101 \cdot 10^{-7}$	-0.501357	6677.32
	$1000 < T \leq 2500$	$7.49936 \cdot 10^{-8}$	-0.317387	6409.92
	$2500 < T \leq 5000$	$4.83064 \cdot 10^{-8}$	-0.264485	6349.28
4 \rightarrow 9	$440 \leq T \leq 1100$	$2.87446 \cdot 10^{-7}$	-0.434330	8217.24
	$1100 < T \leq 5000$	$6.37019 \cdot 10^{-7}$	-0.520453	8494.59
4 \rightarrow 10	$520 \leq T \leq 1500$	$2.54007 \cdot 10^{-7}$	-0.450098	9647.51
	$1500 < T \leq 5000$	$5.21684 \cdot 10^{-7}$	-0.527340	9919.87
4 \rightarrow 11	$600 \leq T \leq 1500$	$3.52393 \cdot 10^{-7}$	-0.548614	10917.4
	$1500 < T \leq 5000$	$5.21684 \cdot 10^{-7}$	-0.527340	9919.87
4 \rightarrow 12	$700 \leq T \leq 2000$	$9.41697 \cdot 10^{-7}$	-0.675116	12596.2
	$2000 < T \leq 5000$	$5.88904 \cdot 10^{-7}$	-0.609756	12639.5
4 \rightarrow 13	$800 \leq T \leq 2000$	$9.80478 \cdot 10^{-9}$	-0.148876	13089.3
	$2000 < T \leq 5000$	$4.90592 \cdot 10^{-7}$	-0.582882	14390.0
4 \rightarrow 14	$900 \leq T \leq 2000$	$2.60260 \cdot 10^{-11}$	0.522764	13703.4
	$2000 < T \leq 5000$	$8.71549 \cdot 10^{-7}$	-0.652413	16809.2

TABLE VIII: Same as table III for $v_i^+ = 5$, as displayed in figure 1, maximal relative deviation of 4.841% and average RMS of 0.0047.

$v_i^+ \rightarrow v_f^+$	Temperature range (K)	A (cm^3/s)	α	B (K)
5 \rightarrow 4	$100 \leq T \leq 1000$	$5.56989 \cdot 10^{-7}$	-0.513528	3.53340
	$1000 < T \leq 2500$	$2.01375 \cdot 10^{-8}$	-0.094742	-436.759
	$2500 < T \leq 5000$	$6.94136 \cdot 10^{-10}$	0.295339	-1236.46
5 \rightarrow 3	$100 \leq T \leq 1000$	$3.10058 \cdot 10^{-7}$	-0.423326	-4.96023
	$1000 < T \leq 5000$	$3.62360 \cdot 10^{-8}$	-0.125478	-116.229
5 \rightarrow 2	$100 \leq T \leq 1000$	$1.06655 \cdot 10^{-7}$	-0.366370	-18.3113
	$1000 < T \leq 5000$	$1.29558 \cdot 10^{-8}$	-0.084856	-152.314
5 \rightarrow 1	$100 \leq T \leq 800$	$5.14091 \cdot 10^{-7}$	-0.521073	-1.52554
	$800 < T \leq 5000$	$4.26149 \cdot 10^{-9}$	0.096789	-537.599
5 \rightarrow 0	$100 \leq T \leq 1000$	$1.48856 \cdot 10^{-7}$	-0.300884	-23.0870
	$1000 < T \leq 5000$	$1.00448 \cdot 10^{-6}$	-0.528422	313.166
5 \rightarrow 6	$100 \leq T \leq 400$	$4.37146 \cdot 10^{-7}$	-0.483497	1694.15
	$400 < T \leq 1500$	$5.91892 \cdot 10^{-7}$	-0.529020	1704.15
	$1500 < T \leq 5000$	$1.05782 \cdot 10^{-9}$	0.225184	472.374
5 \rightarrow 7	$180 \leq T \leq 650$	$1.21009 \cdot 10^{-7}$	0.014402	3269.17
	$650 < T \leq 1700$	$1.21516 \cdot 10^{-7}$	-0.284733	3516.74
	$1700 < T \leq 5000$	$3.54698 \cdot 10^{-8}$	-0.144782	3187.95
5 \rightarrow 8	$260 \leq T \leq 650$	$1.83759 \cdot 10^{-8}$	-0.090440	4793.12
	$650 < T \leq 2100$	$5.73937 \cdot 10^{-9}$	0.059712	4662.73
	$2100 < T \leq 5000$	$7.20070 \cdot 10^{-8}$	-0.224701	5421.46
5 \rightarrow 9	$380 \leq T \leq 1200$	$1.37355 \cdot 10^{-9}$	0.149154	6364.13
	$1200 < T \leq 2500$	$7.66743 \cdot 10^{-10}$	0.222468	6290.03
	$2500 < T \leq 5000$	$6.81228 \cdot 10^{-8}$	-0.279019	7715.95
5 \rightarrow 10	$460 \leq T \leq 900$	$1.73377 \cdot 10^{-10}$	0.440321	7689.34
	$900 < T \leq 2500$	$2.58850 \cdot 10^{-8}$	-0.162749	8416.55
	$2500 < T \leq 5000$	$4.18396 \cdot 10^{-7}$	-0.490630	9309.77
5 \rightarrow 11	$540 \leq T \leq 1000$	$5.21803 \cdot 10^{-10}$	0.299906	9102.53
	$1000 < T \leq 2500$	$5.32106 \cdot 10^{-8}$	-0.265705	9855.20
	$2500 < T \leq 5000$	$6.50276 \cdot 10^{-7}$	-0.546073	10637.9
5 \rightarrow 12	$650 \leq T \leq 1200$	$2.30279 \cdot 10^{-10}$	0.336866	10621.2
	$1200 < T \leq 2500$	$2.45953 \cdot 10^{-8}$	-0.233982	11391.3
	$2500 < T \leq 5000$	$1.56872 \cdot 10^{-7}$	-0.439112	12002.3
5 \rightarrow 13	$750 \leq T \leq 1500$	$2.54628 \cdot 10^{-9}$	-0.031512	12035.7
	$1500 < T \leq 5000$	$2.24958 \cdot 10^{-8}$	-0.279178	12675.0
5 \rightarrow 14	$800 \leq T \leq 2000$	$6.65399 \cdot 10^{-9}$	-0.137991	12985.0
	$2000 < T \leq 5000$	$5.58883 \cdot 10^{-8}$	-0.372194	13735.0
5 \rightarrow 15	$850 \leq T \leq 2500$	$1.04228 \cdot 10^{-9}$	0.084524	13778.2
	$2500 < T \leq 5000$	$1.23324 \cdot 10^{-7}$	-0.444019	15405.9

TABLE IX: Same as table III for $v_i^+ = 6$, as displayed in figure 2, maximal relative deviation of 4.706% and average RMS of 0.0053.

$v_i^+ \rightarrow v_f^+$	Temperature range (K)	A (cm^3/s)	α	B (K)
6 \rightarrow 5	$100 \leq T \leq 900$	$3.70942 \cdot 10^{-7}$	-0.446045	-7.63342
	$900 < T \leq 5000$	$2.79129 \cdot 10^{-8}$	-0.094844	-201.478
6 \rightarrow 4	$100 \leq T \leq 1000$	$3.46289 \cdot 10^{-7}$	-0.467495	-2.18171
	$1000 < T \leq 5000$	$1.47926 \cdot 10^{-8}$	-0.051965	-289.979
6 \rightarrow 3	$100 \leq T \leq 1000$	$2.16284 \cdot 10^{-7}$	-0.451211	-2.10319
	$1000 < T \leq 5000$	$4.54736 \cdot 10^{-9}$	0.054518	-382.150
6 \rightarrow 2	$100 \leq T \leq 1500$	$2.25277 \cdot 10^{-7}$	-0.426085	-8.75750
	$1500 < T \leq 5000$	$2.52568 \cdot 10^{-8}$	-0.154857	-337.870
6 \rightarrow 1	$100 \leq T \leq 800$	$2.50619 \cdot 10^{-7}$	-0.545479	3.32825
	$800 < T \leq 1700$	$8.66864 \cdot 10^{-11}$	0.497744	-808.696
	$1700 < T \leq 5000$	$5.97457 \cdot 10^{-9}$	0.027004	461.581
6 \rightarrow 0	$100 \leq T \leq 1500$	$1.78058 \cdot 10^{-7}$	-0.351516	-13.7935
	$1500 < T \leq 5000$	$2.93734 \cdot 10^{-6}$	-0.688251	503.043
6 \rightarrow 7	$100 \leq T \leq 460$	$4.35370 \cdot 10^{-7}$	-0.408248	1624.97
	$460 < T \leq 5000$	$4.93604 \cdot 10^{-7}$	-0.411277	1691.35
6 \rightarrow 8	$160 \leq T \leq 400$	$5.53976 \cdot 10^{-7}$	-0.466277	3252.76
	$400 < T \leq 1500$	$3.24117 \cdot 10^{-6}$	-0.707137	3392.23
	$1500 < T \leq 5000$	$2.29274 \cdot 10^{-7}$	-0.401535	2749.01
6 \rightarrow 9	$230 \leq T \leq 600$	$2.75278 \cdot 10^{-6}$	-0.672536	4802.44
	$600 < T \leq 2000$	$2.46122 \cdot 10^{-6}$	-0.662899	4763.01
	$2000 < T \leq 5000$	$3.21817 \cdot 10^{-7}$	-0.426979	4277.31
6 \rightarrow 10	$320 \leq T \leq 950$	$9.81810 \cdot 10^{-7}$	-0.663553	6282.91
	$950 < T \leq 5000$	$3.49419 \cdot 10^{-8}$	-0.257514	5717.87
6 \rightarrow 11	$420 \leq T \leq 1300$	$2.12516 \cdot 10^{-8}$	-0.277995	7628.75
	$1300 < T \leq 5000$	$1.97566 \cdot 10^{-9}$	0.006899	7193.40
6 \rightarrow 12	$480 \leq T \leq 5000$	$3.07918 \cdot 10^{-8}$	-0.259332	8791.81
6 \rightarrow 13	$560 \leq T \leq 1500$	$3.83568 \cdot 10^{-9}$	-0.043277	9957.15
	$1500 < T \leq 5000$	$2.59324 \cdot 10^{-8}$	-0.254134	10597.6
6 \rightarrow 14	$650 \leq T \leq 1600$	$9.86322 \cdot 10^{-9}$	-0.214461	11127.2
	$1600 < T \leq 5000$	$1.41149 \cdot 10^{-8}$	-0.245719	11390.3
6 \rightarrow 15	$700 \leq T \leq 1700$	$1.99330 \cdot 10^{-7}$	-0.558820	12607.5
	$1700 < T \leq 5000$	$4.11509 \cdot 10^{-7}$	-0.639626	12839.7
6 \rightarrow 16	$750 \leq T \leq 2000$	$1.80570 \cdot 10^{-7}$	-0.527551	13787.9
	$2000 < T \leq 5000$	$2.31377 \cdot 10^{-6}$	-0.815269	14547.0

TABLE X: Same as table III for $v_i^+ = 7$, as displayed in figure 2, maximal relative deviation of 4.507% and average RMS of 0.0049.

$v_i^+ \rightarrow v_f^+$	Temperature range (K)	A (cm^3/s)	α	B (K)
7 \rightarrow 6	$100 \leq T \leq 5000$	$3.37418 \cdot 10^{-7}$	-0.367396	-16.0055
7 \rightarrow 5	$100 \leq T \leq 700$	$6.89753 \cdot 10^{-8}$	-0.217932	-21.4795
	$700 < T \leq 1700$	$2.20433 \cdot 10^{-7}$	-0.355737	150.159
	$1700 < T \leq 5000$	$2.18723 \cdot 10^{-7}$	-0.362567	50.2353
7 \rightarrow 4	$100 \leq T \leq 900$	$2.28672 \cdot 10^{-7}$	-0.458909	2.53416
	$900 < T \leq 5000$	$1.05626 \cdot 10^{-8}$	-0.037530	-200.131
7 \rightarrow 3	$100 \leq T \leq 700$	$1.05779 \cdot 10^{-7}$	-0.400270	-8.90257
	$700 < T \leq 2000$	$7.32901 \cdot 10^{-9}$	-0.028179	-182.674
	$2000 < T \leq 5000$	$2.22962 \cdot 10^{-7}$	-0.428072	577.902
7 \rightarrow 2	$100 \leq T \leq 1500$	$4.48329 \cdot 10^{-7}$	-0.529847	14.8007
	$1500 < T \leq 5000$	$2.83299 \cdot 10^{-9}$	0.085167	-826.414
7 \rightarrow 1	$100 \leq T \leq 700$	$1.00443 \cdot 10^{-7}$	-0.386590	-10.0161
	$700 < T \leq 1700$	$9.68579 \cdot 10^{-10}$	0.240321	-398.928
	$1700 < T \leq 5000$	$1.28210 \cdot 10^{-7}$	-0.323788	789.265
7 \rightarrow 0	$100 \leq T \leq 1000$	$2.23629 \cdot 10^{-7}$	-0.439551	4.12887
	$1000 < T \leq 5000$	$5.92475 \cdot 10^{-7}$	-0.553455	189.878
7 \rightarrow 8	$100 \leq T \leq 400$	$6.80708 \cdot 10^{-7}$	-0.392035	1590.04
	$400 < T \leq 1000$	$4.87541 \cdot 10^{-6}$	-0.667102	1721.04
	$1000 < T \leq 5000$	$1.47057 \cdot 10^{-6}$	-0.531807	1429.38
7 \rightarrow 9	$160 \leq T \leq 400$	$1.37265 \cdot 10^{-6}$	-0.709983	3138.77
	$400 < T \leq 1000$	$1.75384 \cdot 10^{-7}$	-0.428938	2981.03
	$1000 < T \leq 5000$	$1.58164 \cdot 10^{-8}$	-0.127625	2640.45
7 \rightarrow 10	$240 \leq T \leq 700$	$2.95504 \cdot 10^{-8}$	-0.146963	4487.15
	$700 < T \leq 5000$	$3.18819 \cdot 10^{-7}$	-0.444849	4811.26
7 \rightarrow 11	$320 \leq T \leq 1000$	$2.63726 \cdot 10^{-7}$	-0.512544	6088.15
	$1000 < T \leq 5000$	$4.07183 \cdot 10^{-8}$	-0.294606	5560.91
7 \rightarrow 12	$400 \leq T \leq 1000$	$2.14375 \cdot 10^{-7}$	-0.573817	7364.27
	$1000 < T \leq 2500$	$6.02160 \cdot 10^{-8}$	-0.422393	7123.42
	$2500 < T \leq 5000$	$8.85182 \cdot 10^{-10}$	0.054397	5893.89
7 \rightarrow 13	$460 \leq T \leq 1400$	$3.46987 \cdot 10^{-7}$	-0.600761	8655.21
	$1400 < T \leq 5000$	$5.22711 \cdot 10^{-9}$	-0.109419	7716.82
7 \rightarrow 14	$560 \leq T \leq 1500$	$4.47577 \cdot 10^{-8}$	-0.348135	9650.12
	$1500 < T \leq 5000$	$8.57693 \cdot 10^{-9}$	-0.151472	9339.79
7 \rightarrow 15	$600 \leq T \leq 2000$	$4.05949 \cdot 10^{-9}$	-0.109537	10670.0
	$2000 < T \leq 5000$	$4.20558 \cdot 10^{-9}$	-0.106801	10810.7
7 \rightarrow 16	$700 \leq T \leq 1000$	$1.17187 \cdot 10^{-7}$	-0.559309	12044.6
	$1000 < T \leq 5000$	$4.20426 \cdot 10^{-9}$	-0.166911	11348.1
7 \rightarrow 17	$700 \leq T \leq 1000$	$8.31094 \cdot 10^{-7}$	-0.762056	13081.4
	$1000 < T \leq 5000$	$2.65219 \cdot 10^{-7}$	-0.630184	12803.8

TABLE XI: Same as table III for $v_i^+ = 8$, as displayed in figure 2, maximal relative deviation of 3.697% and average RMS of 0.0054.

$v_i^+ \rightarrow v_f^+$	Temperature range (K)	A (cm^3/s)	α	B (K)
8 \rightarrow 7	$100 \leq T \leq 500$	$5.78241 \cdot 10^{-7}$	-0.536410	2.54953
	$500 < T \leq 1500$	$6.89449 \cdot 10^{-6}$	-0.712737	172.842
	$1500 < T \leq 5000$	$8.52219 \cdot 10^{-7}$	-0.471517	-331.533
8 \rightarrow 6	$100 \leq T \leq 500$	$3.16466 \cdot 10^{-7}$	-0.383842	10.6386
	$500 < T \leq 1500$	$2.60307 \cdot 10^{-6}$	-0.679387	149.899
	$1500 < T \leq 5000$	$2.87412 \cdot 10^{-7}$	-0.426602	-396.479
8 \rightarrow 5	$100 \leq T \leq 500$	$1.63510 \cdot 10^{-7}$	-0.325893	-8.18654
	$500 < T \leq 1500$	$4.22095 \cdot 10^{-7}$	-0.450519	79.3021
	$1500 < T \leq 5000$	$3.29429 \cdot 10^{-7}$	-0.427530	-41.4880
8 \rightarrow 4	$100 \leq T \leq 500$	$3.37039 \cdot 10^{-7}$	-0.502840	8.13046
	$500 < T \leq 1500$	$3.27948 \cdot 10^{-7}$	-0.495167	16.8707
	$1500 < T \leq 5000$	$3.56897 \cdot 10^{-8}$	-0.231563	-423.381
8 \rightarrow 3	$100 \leq T \leq 500$	$1.04359 \cdot 10^{-7}$	-0.321301	-18.8331
	$500 < T \leq 1500$	$3.17592 \cdot 10^{-8}$	-0.142575	-61.4199
	$1500 < T \leq 5000$	$9.16946 \cdot 10^{-7}$	-0.548129	547.126
8 \rightarrow 2	$100 \leq T \leq 500$	$3.85687 \cdot 10^{-7}$	-0.677221	17.1568
	$500 < T \leq 1500$	$2.62968 \cdot 10^{-9}$	-0.003202	-388.783
	$1500 < T \leq 5000$	$6.05370 \cdot 10^{-10}$	0.223618	-62.8571
8 \rightarrow 1	$100 \leq T \leq 500$	$5.19264 \cdot 10^{-8}$	-0.324035	-18.0165
	$500 < T \leq 1500$	$5.95451 \cdot 10^{-10}$	0.293257	-341.671
	$1500 < T \leq 5000$	$5.95451 \cdot 10^{-10}$	0.293257	-341.671
8 \rightarrow 0	$100 \leq T \leq 500$	$3.09423 \cdot 10^{-7}$	-0.536410	2.54953
	$500 < T \leq 1500$	$2.19437 \cdot 10^{-7}$	-0.486125	-14.5982
	$1500 < T \leq 5000$	$2.04734 \cdot 10^{-7}$	-0.475431	2.70393
8 \rightarrow 9	$100 \leq T \leq 400$	$9.49750 \cdot 10^{-7}$	-0.530662	1516.89
	$400 < T \leq 1000$	$2.83633 \cdot 10^{-7}$	-0.359254	1443.77
	$1000 < T \leq 5000$	$4.07622 \cdot 10^{-7}$	-0.413605	1410.77
8 \rightarrow 10	$170 \leq T \leq 400$	$4.15169 \cdot 10^{-10}$	0.325430	2808.01
	$400 < T \leq 1000$	$3.35729 \cdot 10^{-9}$	0.048405	2993.08
	$1000 < T \leq 5000$	$5.58929 \cdot 10^{-9}$	-0.035381	2866.01
8 \rightarrow 11	$240 \leq T \leq 400$	$5.35457 \cdot 10^{-7}$	-0.569165	4472.53
	$400 < T \leq 1000$	$2.73894 \cdot 10^{-7}$	-0.477771	4420.27
	$1000 < T \leq 5000$	$9.80430 \cdot 10^{-8}$	-0.357002	4192.51
8 \rightarrow 12	$320 \leq T \leq 400$	$1.35568 \cdot 10^{-7}$	-0.449477	5765.65
	$400 < T \leq 1000$	$9.19102 \cdot 10^{-8}$	-0.396388	5735.52
	$1000 < T \leq 5000$	$2.88488 \cdot 10^{-8}$	-0.266229	5409.83
8 \rightarrow 13	$400 \leq T \leq 1000$	$1.47058 \cdot 10^{-7}$	-0.527347	6967.98
	$1000 < T \leq 5000$	$5.13127 \cdot 10^{-9}$	-0.152644	5990.70
	8 \rightarrow 14	$480 \leq T \leq 1000$	$2.18512 \cdot 10^{-7}$	-0.589139
8 \rightarrow 15	$1000 < T \leq 5000$	$1.39150 \cdot 10^{-9}$	-0.014322	7001.90
	8 \rightarrow 15	$520 \leq T \leq 1000$	$1.63717 \cdot 10^{-6}$	-0.807889
8 \rightarrow 16	$1000 < T \leq 5000$	$4.53125 \cdot 10^{-9}$	-0.117374	8117.49
	8 \rightarrow 16	$600 \leq T \leq 1000$	$5.91540 \cdot 10^{-7}$	-0.706951
8 \rightarrow 17	$1000 < T \leq 5000$	$2.64262 \cdot 10^{-9}$	-0.062595	9368.17
	8 \rightarrow 17	$700 \leq T \leq 1000$	$3.30687 \cdot 10^{-8}$	-0.442046
8 \rightarrow 18	$1000 < T \leq 5000$	$3.21768 \cdot 10^{-10}$	0.127603	10540.1
	8 \rightarrow 18	$750 \leq T \leq 1000$	$2.60829 \cdot 10^{-9}$	-0.174712
	$1000 < T \leq 5000$	$3.60844 \cdot 10^{-10}$	0.068440	12019.2

TABLE XII: Same as table III for $v_i^+ = 9$, as displayed in figure 2, maximal relative deviation of 4.062% and average RMS of 0.0038.

$v_i^+ \rightarrow v_f^+$	Temperature range (K)	A (cm^3/s)	α	B (K)
9 \rightarrow 8	$100 \leq T \leq 500$	$1.44871 \cdot 10^{-6}$	-0.593333	-1.62306
	$500 < T \leq 1500$	$3.65915 \cdot 10^{-7}$	-0.392892	-69.8892
	$1500 < T \leq 5000$	$2.67847 \cdot 10^{-7}$	-0.367149	-264.834
9 \rightarrow 7	$100 \leq T \leq 500$	$1.24170 \cdot 10^{-6}$	-0.695805	14.5189
	$500 < T \leq 1500$	$9.79737 \cdot 10^{-8}$	-0.351667	-189.513
	$1500 < T \leq 5000$	$1.44986 \cdot 10^{-8}$	-0.117823	-505.359
9 \rightarrow 6	$100 \leq T \leq 500$	$1.24407 \cdot 10^{-6}$	-0.558619	4.63465
	$500 < T \leq 1500$	$3.89262 \cdot 10^{-6}$	-0.719476	76.8211
	$1500 < T \leq 5000$	$4.21510 \cdot 10^{-7}$	-0.456587	-381.530
9 \rightarrow 5	$100 \leq T \leq 500$	$2.06640 \cdot 10^{-7}$	-0.448587	-18.4794
	$500 < T \leq 1500$	$2.17823 \cdot 10^{-6}$	-0.766914	168.897
	$1500 < T \leq 5000$	$1.99507 \cdot 10^{-8}$	-0.218426	-872.766
9 \rightarrow 4	$100 \leq T \leq 500$	$1.70925 \cdot 10^{-7}$	-0.362443	-9.96986
	$500 < T \leq 1500$	$2.95153 \cdot 10^{-7}$	-0.437449	29.4370
	$1500 < T \leq 5000$	$4.01500 \cdot 10^{-7}$	-0.469641	143.683
9 \rightarrow 3	$100 \leq T \leq 500$	$4.32221 \cdot 10^{-8}$	-0.188273	-24.1836
	$500 < T \leq 1500$	$4.48697 \cdot 10^{-7}$	-0.502495	171.029
	$1500 < T \leq 5000$	$2.22533 \cdot 10^{-7}$	-0.426892	-50.0461
9 \rightarrow 2	$100 \leq T \leq 500$	$1.02774 \cdot 10^{-7}$	-0.483004	-7.30020
	$500 < T \leq 1500$	$3.06525 \cdot 10^{-10}$	0.330319	-395.902
	$1500 < T \leq 5000$	$3.26279 \cdot 10^{-8}$	-0.208900	725.828
9 \rightarrow 1	$100 \leq T \leq 500$	$8.86504 \cdot 10^{-8}$	-0.420146	-9.85374
	$500 < T \leq 1500$	$3.83639 \cdot 10^{-10}$	0.322306	-430.712
	$1500 < T \leq 5000$	$4.67244 \cdot 10^{-7}$	-0.502120	1216.24
9 \rightarrow 0	$100 \leq T \leq 500$	$1.38755 \cdot 10^{-7}$	-0.446860	-6.22064
	$500 < T \leq 1500$	$1.72365 \cdot 10^{-7}$	-0.481270	-3.16788
	$1500 < T \leq 5000$	$7.12289 \cdot 10^{-8}$	-0.369724	-100.655
9 \rightarrow 10	$100 \leq T \leq 400$	$1.20071 \cdot 10^{-7}$	-0.234322	1439.04
	$400 < T \leq 1000$	$4.95822 \cdot 10^{-7}$	-0.430412	1539.01
	$1000 < T \leq 5000$	$6.58499 \cdot 10^{-7}$	-0.479700	1459.11
9 \rightarrow 11	$160 \leq T \leq 400$	$2.11543 \cdot 10^{-7}$	-0.466053	2885.60
	$400 < T \leq 1000$	$1.24949 \cdot 10^{-7}$	-0.388771	2861.73
	$1000 < T \leq 5000$	$3.20005 \cdot 10^{-8}$	-0.239367	2473.46
9 \rightarrow 12	$230 \leq T \leq 400$	$2.59073 \cdot 10^{-7}$	-0.528059	4271.87
	$400 < T \leq 1000$	$2.59555 \cdot 10^{-7}$	-0.531444	4261.73
	$1000 < T \leq 5000$	$8.74783 \cdot 10^{-9}$	-0.125368	3613.08
9 \rightarrow 13	$300 \leq T \leq 400$	$1.85508 \cdot 10^{-7}$	-0.474054	5459.09
	$400 < T \leq 1000$	$2.46768 \cdot 10^{-7}$	-0.512874	5481.55
	$1000 < T \leq 5000$	$3.72732 \cdot 10^{-8}$	-0.290945	5066.43
9 \rightarrow 14	$400 \leq T \leq 1000$	$4.04717 \cdot 10^{-7}$	-0.676035	6685.63
	$1000 < T \leq 5000$	$1.88103 \cdot 10^{-9}$	-0.047674	5464.71
9 \rightarrow 15	$460 \leq T \leq 1000$	$8.55868 \cdot 10^{-8}$	-0.523497	7733.14
	$1000 < T \leq 5000$	$5.12315 \cdot 10^{-10}$	0.058287	6354.33
9 \rightarrow 16	$520 \leq T \leq 1000$	$9.83633 \cdot 10^{-8}$	-0.505568	8961.72
	$1000 < T \leq 5000$	$1.71131 \cdot 10^{-9}$	-0.044699	7889.40
9 \rightarrow 17	$560 \leq T \leq 1000$	$3.44385 \cdot 10^{-7}$	-0.645044	9929.37
	$1000 < T \leq 5000$	$2.87160 \cdot 10^{-9}$	-0.084483	8860.52
9 \rightarrow 18	$650 \leq T \leq 1000$	$3.83691 \cdot 10^{-7}$	-0.693580	10839.3
	$1000 < T \leq 5000$	$9.37271 \cdot 10^{-10}$	0.022107	9636.56
9 \rightarrow 19	$650 \leq T \leq 1000$	$6.27368 \cdot 10^{-8}$	-0.562797	11532.9
	$1000 < T \leq 5000$	$1.85441 \cdot 10^{-14}$	1.152320	7032.37

TABLE XIII: Same as table III for $v_i^+ = 10$, as displayed in figure 2, maximal relative deviation of 3.541% and average RMS of 0.0038.

$v_i^+ \rightarrow v_f^+$	Temperature range (K)	A (cm^3/s)	α	B (K)
10 \rightarrow 9	$100 \leq T \leq 500$	$1.92577 \cdot 10^{-7}$	-0.305078	-26.8405
	$500 < T \leq 1500$	$9.22604 \cdot 10^{-7}$	-0.512261	111.699
	$1500 < T \leq 5000$	$4.18158 \cdot 10^{-7}$	-0.429462	-175.701
10 \rightarrow 8	$100 \leq T \leq 650$	$1.10611 \cdot 10^{-8}$	-0.160095	-66.0942
	$650 < T \leq 1500$	$6.14458 \cdot 10^{-9}$	-0.031534	25.8044
	$1500 < T \leq 5000$	$4.20322 \cdot 10^{-9}$	-0.003797	-252.871
10 \rightarrow 7	$100 \leq T \leq 500$	$1.73636 \cdot 10^{-7}$	-0.401646	-18.5255
	$500 < T \leq 1500$	$4.87697 \cdot 10^{-8}$	-0.213395	-71.3638
	$1500 < T \leq 5000$	$3.15820 \cdot 10^{-7}$	-0.443674	207.158
10 \rightarrow 6	$100 \leq T \leq 500$	$3.60732 \cdot 10^{-7}$	-0.516145	-1.65344
	$500 < T \leq 1500$	$7.79404 \cdot 10^{-7}$	-0.632888	23.7802
	$1500 < T \leq 5000$	$3.27638 \cdot 10^{-8}$	-0.250421	-543.330
10 \rightarrow 5	$100 \leq T \leq 500$	$3.52024 \cdot 10^{-7}$	-0.460535	15.1393
	$500 < T \leq 1500$	$4.77314 \cdot 10^{-6}$	-0.839672	147.701
	$1500 < T \leq 5000$	$3.13883 \cdot 10^{-8}$	-0.234609	-763.686
10 \rightarrow 4	$100 \leq T \leq 500$	$1.80921 \cdot 10^{-7}$	-0.387829	-0.99888
	$500 < T \leq 1500$	$3.81103 \cdot 10^{-7}$	-0.501019	22.6404
	$1500 < T \leq 5000$	$2.89393 \cdot 10^{-7}$	-0.462745	31.7006
10 \rightarrow 3	$100 \leq T \leq 500$	$7.58313 \cdot 10^{-8}$	-0.281289	-20.6885
	$500 < T \leq 1500$	$2.03004 \cdot 10^{-6}$	-0.736521	210.870
	$1500 < T \leq 5000$	$5.68021 \cdot 10^{-8}$	-0.308307	-456.762
10 \rightarrow 2	$100 \leq T \leq 500$	$7.31922 \cdot 10^{-9}$	-0.067803	-46.7249
	$500 < T \leq 1500$	$1.09392 \cdot 10^{-8}$	-0.109858	20.2654
	$1500 < T \leq 5000$	$2.86504 \cdot 10^{-8}$	-0.217551	302.217
10 \rightarrow 1	$100 \leq T \leq 500$	$1.77418 \cdot 10^{-7}$	-0.501015	3.90605
	$500 < T \leq 1500$	$1.64880 \cdot 10^{-9}$	0.142933	-339.635
	$1500 < T \leq 5000$	$1.89084 \cdot 10^{-6}$	-0.683998	1184.11
10 \rightarrow 0	$100 \leq T \leq 500$	$1.13041 \cdot 10^{-7}$	-0.456875	0.21805
	$500 < T \leq 1500$	$4.54531 \cdot 10^{-8}$	-0.330801	-65.4893
	$1500 < T \leq 5000$	$4.86730 \cdot 10^{-8}$	-0.327513	84.7081
10 \rightarrow 11	$100 \leq T \leq 400$	$2.78742 \cdot 10^{-7}$	-0.356049	1385.68
	$400 < T \leq 1000$	$4.46097 \cdot 10^{-7}$	-0.419660	1422.69
	$1000 < T \leq 5000$	$8.10946 \cdot 10^{-7}$	-0.501366	1445.19
10 \rightarrow 12	$140 \leq T \leq 400$	$2.13203 \cdot 10^{-6}$	-0.753681	2786.00
	$400 < T \leq 1000$	$1.04984 \cdot 10^{-6}$	-0.655861	2735.17
	$1000 < T \leq 5000$	$8.91478 \cdot 10^{-8}$	-0.359020	2283.81
10 \rightarrow 13	$230 \leq T \leq 400$	$4.10433 \cdot 10^{-8}$	-0.373744	4005.04
	$400 < T \leq 1000$	$2.41232 \cdot 10^{-8}$	-0.306044	3948.51
	$1000 < T \leq 5000$	$5.04050 \cdot 10^{-10}$	0.163101	3267.37
10 \rightarrow 14	$290 \leq T \leq 400$	$1.06117 \cdot 10^{-7}$	-0.419498	5166.32
	$400 < T \leq 1000$	$1.19855 \cdot 10^{-7}$	-0.434089	5182.09
	$1000 < T \leq 5000$	$3.45317 \cdot 10^{-8}$	-0.289256	4896.40
10 \rightarrow 15	$360 \leq T \leq 400$	$1.94581 \cdot 10^{-7}$	-0.578360	6313.66
	$400 < T \leq 1000$	$1.77365 \cdot 10^{-7}$	-0.569324	6293.84
	$1000 < T \leq 5000$	$2.27823 \cdot 10^{-9}$	-0.053242	5386.11
10 \rightarrow 16	$420 \leq T \leq 1000$	$2.65598 \cdot 10^{-7}$	-0.688741	7328.40
	$1000 < T \leq 5000$	$2.90340 \cdot 10^{-10}$	0.103411	5706.67
	$500 \leq T \leq 1000$	$1.33379 \cdot 10^{-8}$	-0.315155	8238.91
10 \rightarrow 17	$1000 < T \leq 5000$	$3.48882 \cdot 10^{-10}$	0.090272	7160.36
	$560 \leq T \leq 1000$	$4.78249 \cdot 10^{-8}$	-0.444997	9369.07
	$1000 < T \leq 5000$	$1.08039 \cdot 10^{-9}$	-0.010176	8414.03
10 \rightarrow 18	$600 \leq T \leq 1000$	$1.51702 \cdot 10^{-7}$	-0.584259	10253.4
	$1000 < T \leq 5000$	$1.50933 \cdot 10^{-9}$	-0.040020	9279.58
	$1000 < T \leq 5000$	$1.51702 \cdot 10^{-7}$	-0.584259	10253.4
10 \rightarrow 19	$600 \leq T \leq 1000$	$1.51702 \cdot 10^{-7}$	-0.584259	10253.4
	$1000 < T \leq 5000$	$1.50933 \cdot 10^{-9}$	-0.040020	9279.58
10 \rightarrow 20	$600 \leq T \leq 1000$	$1.51702 \cdot 10^{-7}$	-0.584259	10253.4
	$1000 < T \leq 5000$	$1.50933 \cdot 10^{-9}$	-0.040020	9279.58

TABLE XIV: Isotopic effects: Dissociative recombination rate coefficient of the BeH^+ , BeD^+ and BeT^+ molecular cations as function of the energy of the initial vibrational level of the target $E_{v_i^+} - E_0$ (relative to the ground vibrational level) for two electron temperatures: 300 K and 1000 K.

Temperature (K)	BeH^+			BeD^+			BeT^+		
	v_i^+	$E_{v_i^+} - E_0$ (eV)	Rate coefficient (cm^3/s)	v_i^+	$E_{v_i^+} - E_0$ (eV)	Rate coefficient (cm^3/s)	v_i^+	$E_{v_i^+} - E_0$ (eV)	Rate coefficient (cm^3/s)
300	0	0.000	$1.13043 \cdot 10^{-7}$	0	0.000	$1.26201 \cdot 10^{-7}$	0	0.000	$1.34068 \cdot 10^{-7}$
	1	0.259	$1.89605 \cdot 10^{-7}$	1	0.194	$2.13453 \cdot 10^{-7}$	1	0.167	$2.15156 \cdot 10^{-7}$
	2	0.507	$2.55119 \cdot 10^{-7}$	2	0.381	$2.25027 \cdot 10^{-7}$	2	0.327	$2.23157 \cdot 10^{-7}$
	3	0.746	$2.05097 \cdot 10^{-7}$	3	0.565	$2.34042 \cdot 10^{-7}$	3	0.486	$3.20841 \cdot 10^{-7}$
	4	0.975	$2.35437 \cdot 10^{-7}$	4	0.743	$2.41174 \cdot 10^{-7}$	4	0.641	$2.09956 \cdot 10^{-7}$
	5	1.191	$4.54551 \cdot 10^{-7}$	5	0.915	$1.81772 \cdot 10^{-7}$	5	0.792	$1.947060 \cdot 10^{-7}$
	6	1.396	$2.24184 \cdot 10^{-7}$	6	1.080	$2.93495 \cdot 10^{-7}$	6	0.937	$1.996350 \cdot 10^{-7}$
	7	1.588	$1.64762 \cdot 10^{-7}$	7	1.238	$3.67180 \cdot 10^{-7}$	7	1.078	$2.752180 \cdot 10^{-7}$
	8	1.762	$1.55939 \cdot 10^{-7}$	8	1.391	$2.48675 \cdot 10^{-7}$	8	1.214	$3.978330 \cdot 10^{-7}$
	9	1.921	$1.38102 \cdot 10^{-7}$	9	1.538	$2.19837 \cdot 10^{-7}$	9	1.347	$2.280440 \cdot 10^{-7}$
	10	2.066	$1.08544 \cdot 10^{-7}$	10	1.675	$1.84860 \cdot 10^{-7}$	10	1.475	$1.922060 \cdot 10^{-7}$
	11	2.198	$1.04839 \cdot 10^{-7}$	11	1.802	$1.53598 \cdot 10^{-7}$	11	1.597	$1.624550 \cdot 10^{-7}$
	12	2.316	$0.90535 \cdot 10^{-7}$	12	1.921	$1.403460 \cdot 10^{-7}$	12	1.712	$1.636260 \cdot 10^{-7}$
	13	2.418	$0.71285 \cdot 10^{-7}$	13	2.031	$1.289540 \cdot 10^{-7}$	13	1.819	$1.462200 \cdot 10^{-7}$
	14	2.503	$0.56714 \cdot 10^{-7}$	14	2.135	$1.184330 \cdot 10^{-7}$	14	1.921	$1.264430 \cdot 10^{-7}$
	15	2.568	$0.38451 \cdot 10^{-7}$	15	2.232	$0.1065160 \cdot 10^{-7}$	15	2.017	$1.224940 \cdot 10^{-7}$
	16	2.614	$0.248093 \cdot 10^{-7}$	16	2.321	$0.942660 \cdot 10^{-7}$	16	2.107	$1.131190 \cdot 10^{-7}$
	17	2.646	$0.12415 \cdot 10^{-7}$	17	2.401	$0.688125 \cdot 10^{-7}$	17	2.193	$1.140570 \cdot 10^{-7}$
				18	2.473	$0.664439 \cdot 10^{-7}$	18	2.273	$1.05216 \cdot 10^{-7}$
				19	2.535	$0.53440 \cdot 10^{-7}$	19	2.348	$0.98783 \cdot 10^{-7}$
				20	2.586	$0.38638 \cdot 10^{-7}$	20	2.416	$0.91899 \cdot 10^{-7}$
				21	2.624	$0.26081 \cdot 10^{-7}$	21	2.477	$0.78952 \cdot 10^{-7}$
				22	2.656	$0.35449 \cdot 10^{-7}$	22	2.532	$0.68255 \cdot 10^{-7}$
				23	2.679	$0.38637 \cdot 10^{-7}$	23	2.578	$0.55167 \cdot 10^{-7}$
							24	2.617	$0.42227 \cdot 10^{-7}$
							25	2.648	$0.37486 \cdot 10^{-7}$
							26	2.673	$0.28288 \cdot 10^{-7}$
						27	2.693	$0.15356 \cdot 10^{-7}$	
1000	0	0.000	$0.62273 \cdot 10^{-7}$	0	0.000	$0.6676 \cdot 10^{-7}$	0	0.000	$0.66745 \cdot 10^{-7}$
	1	0.259	$1.15746 \cdot 10^{-7}$	1	0.194	$1.15668 \cdot 10^{-7}$	1	0.167	$1.08648 \cdot 10^{-7}$
	2	0.507	$1.48471 \cdot 10^{-7}$	2	0.381	$1.49232 \cdot 10^{-7}$	2	0.327	$1.3651 \cdot 10^{-7}$
	3	0.746	$1.23833 \cdot 10^{-7}$	3	0.565	$1.42339 \cdot 10^{-7}$	3	0.486	$1.79330 \cdot 10^{-7}$
	4	0.975	$1.59735 \cdot 10^{-7}$	4	0.743	$1.49176 \cdot 10^{-7}$	4	0.641	$1.47070 \cdot 10^{-7}$
	5	1.191	$2.37894 \cdot 10^{-7}$	5	0.915	$1.26522 \cdot 10^{-7}$	5	0.792	$1.22328 \cdot 10^{-7}$
	6	1.396	$1.54019 \cdot 10^{-7}$	6	1.080	$1.97732 \cdot 10^{-7}$	6	0.937	$1.29393 \cdot 10^{-7}$
	7	1.588	$1.02440 \cdot 10^{-7}$	7	1.238	$1.81918 \cdot 10^{-7}$	7	1.078	$1.88718 \cdot 10^{-7}$
	8	1.762	$0.91984 \cdot 10^{-7}$	8	1.391	$1.46238 \cdot 10^{-7}$	8	1.214	$2.03371 \cdot 10^{-7}$
	9	1.921	$0.81237 \cdot 10^{-7}$	9	1.538	$1.25893 \cdot 10^{-7}$	9	1.347	$1.39099 \cdot 10^{-7}$
	10	2.066	$0.66003 \cdot 10^{-7}$	10	1.675	$1.04380 \cdot 10^{-7}$	10	1.475	$1.23618 \cdot 10^{-7}$
	11	2.198	$0.65134 \cdot 10^{-7}$	11	1.802	$0.89330 \cdot 10^{-7}$	11	1.597	$1.05604 \cdot 10^{-7}$
	12	2.316	$0.54343 \cdot 10^{-7}$	12	1.921	$0.81329 \cdot 10^{-7}$	12	1.712	$0.980590 \cdot 10^{-7}$
	13	2.418	$0.43323 \cdot 10^{-7}$	13	2.031	$0.73243 \cdot 10^{-7}$	13	1.819	$0.86606 \cdot 10^{-7}$
	14	2.503	$0.33629 \cdot 10^{-7}$	14	2.135	$0.66925 \cdot 10^{-7}$	14	1.921	$0.77773 \cdot 10^{-7}$
	15	2.568	$0.22762 \cdot 10^{-7}$	15	2.232	$0.59011 \cdot 10^{-7}$	15	2.017	$0.71660 \cdot 10^{-7}$
	16	2.614	$0.15309 \cdot 10^{-7}$	16	2.321	$0.51745 \cdot 10^{-7}$	16	2.107	$0.66103 \cdot 10^{-7}$
	17	2.646	$0.12415 \cdot 10^{-7}$	17	2.401	$0.37836 \cdot 10^{-7}$	17	2.193	$0.62597 \cdot 10^{-7}$
				18	2.473	$0.36924 \cdot 10^{-7}$	18	2.273	$0.57802 \cdot 10^{-7}$
				19	2.535	$0.30333 \cdot 10^{-7}$	19	2.348	$0.52977 \cdot 10^{-7}$
				20	2.586	$0.22249 \cdot 10^{-7}$	20	2.416	$0.48865 \cdot 10^{-7}$
				21	2.624	$0.32560 \cdot 10^{-7}$	21	2.477	$0.42874 \cdot 10^{-7}$
				22	2.656	$0.36031 \cdot 10^{-7}$	22	2.532	$0.36855 \cdot 10^{-7}$
				23	2.679	$0.22243 \cdot 10^{-7}$	23	2.578	$0.29787 \cdot 10^{-7}$
							24	2.617	$0.23348 \cdot 10^{-7}$
							25	2.648	$0.21063 \cdot 10^{-7}$
							26	2.673	$0.16473 \cdot 10^{-7}$
						27	2.693	$0.09307 \cdot 10^{-7}$	

TABLE XV: Same as table XIV for 5000 K electron temperature.

Temperature (K)	BeH ⁺			BeD ⁺			BeT ⁺		
	v_i^+	$E_{v_i^+} - E_0$ (eV)	Rate coefficient (cm ³ /s)	v_i^+	$E_{v_i^+} - E_0$ (eV)	Rate coefficient (cm ³ /s)	v_i^+	$E_{v_i^+} - E_0$ (eV)	Rate coefficient (cm ³ /s)
5000	0	0.000	0.55998·10 ⁻⁷	0	0.000	0.37608·10 ⁻⁷	0	0.000	0.29001·10 ⁻⁷
	1	0.259	0.82794·10 ⁻⁷	1	0.194	0.65690·10 ⁻⁷	1	0.167	0.51597·10 ⁻⁷
	2	0.507	0.77280·10 ⁻⁷	2	0.381	0.80984·10 ⁻⁷	2	0.327	0.73925·10 ⁻⁷
	3	0.746	0.79359·10 ⁻⁷	3	0.565	0.72617·10 ⁻⁷	3	0.486	0.75943·10 ⁻⁷
	4	0.975	0.92771·10 ⁻⁷	4	0.743	0.77806·10 ⁻⁷	4	0.641	0.74990·10 ⁻⁷
	5	1.191	0.96326·10 ⁻⁷	5	0.915	0.81876·10 ⁻⁷	5	0.792	0.71843·10 ⁻⁷
	6	1.396	0.79917·10 ⁻⁷	6	1.080	0.96890·10 ⁻⁷	6	0.937	0.79576·10 ⁻⁷
	7	1.588	0.56721·10 ⁻⁷	7	1.238	0.84272·10 ⁻⁷	7	1.078	0.92157·10 ⁻⁷
	8	1.762	0.51647·10 ⁻⁷	8	1.391	0.75447·10 ⁻⁷	8	1.214	0.86090·10 ⁻⁷
	9	1.921	0.46885·10 ⁻⁷	9	1.538	0.65267·10 ⁻⁷	9	1.347	0.74701·10 ⁻⁷
	10	2.066	0.36131·10 ⁻⁷	10	1.675	0.55439·10 ⁻⁷	10	1.475	0.68115·10 ⁻⁷
	11	2.198	0.36483·10 ⁻⁷	11	1.802	0.49067·10 ⁻⁷	11	1.597	0.58977·10 ⁻⁷
	12	2.316	0.30467·10 ⁻⁷	12	1.921	0.44263·10 ⁻⁷	12	1.712	0.52260·10 ⁻⁷
	13	2.418	0.25328·10 ⁻⁷	13	2.031	0.39992·10 ⁻⁷	13	1.819	0.47411·10 ⁻⁷
	14	2.503	0.20608·10 ⁻⁷	14	2.135	0.36903·10 ⁻⁷	14	1.921	0.43223·10 ⁻⁷
	15	2.568	0.14556·10 ⁻⁷	15	2.232	0.33269·10 ⁻⁷	15	2.017	0.40022·10 ⁻⁷
	16	2.614	0.10140·10 ⁻⁷	16	2.321	0.29882·10 ⁻⁷	16	2.107	0.37307·10 ⁻⁷
	17	2.646	0.053571·10 ⁻⁷	17	2.401	0.21835·10 ⁻⁷	17	2.193	0.34827·10 ⁻⁷
				18	2.473	0.22794·10 ⁻⁷	18	2.273	0.32048·10 ⁻⁷
				19	2.535	0.19643·10 ⁻⁷	19	2.348	0.29209·10 ⁻⁷
				20	2.586	0.15036·10 ⁻⁷	20	2.416	0.27011·10 ⁻⁷
				21	2.624	0.18515·10 ⁻⁷	21	2.477	0.24116·10 ⁻⁷
				22	2.656	0.19536·10 ⁻⁷	22	2.532	0.21027·10 ⁻⁷
				23	2.679	0.15037·10 ⁻⁷	23	2.578	0.17552·10 ⁻⁷
							24	2.617	0.14177·10 ⁻⁷
							25	2.648	0.13063·10 ⁻⁷
							26	2.673	0.10503·10 ⁻⁷
							27	2.693	0.06095·10 ⁻⁷